# Chapter 7

# Discussion

This chapter is a discussion of inertial and particle concentration effects for the experiments with a matched density, followed by direct comparisons of the torque measurements with different density ratios. In the previous chapter the effective volume fraction was measured with the help of the flow visualization. Such measurements are used to predict the effective volume fraction of mixtures with a density ratio of $\rho_p/\rho = 1.05$. It is hypothesized that the effective relative viscosity for flows with a mismatch density is equal to the effective relative viscosity for flows with a match density as long as both cases have the same effective volume fraction. This hypothesis is based on the results for mixtures with a matched density, where for $\phi > 30$ the effective relative viscosity does not appear to vary dramatically with the Stokes number but it strongly depends on the volume fraction.

## 7.1 Inertial and particle concentration effects on mixtures with $\rho_p/\rho = 1$

In Section 4.2 it was shown that the effective relative viscosity for experiments with a liquid with matched density and volume fractions of 10, 20, and 30% exhibit a dependance on Stokes number, (see Figure 4.3). To study if this dependance can be attributed to the presence of particles or to the hydrodynamic inertial effects, a comparison between the normalized torques for the mixture and for the suspending liquid is made as a function of the gap Reynolds number as defined in equation 2.5. Figure 7.1 shows the measured torques normalized by the theoretical laminar torque for volume fractions of 10, 20, and 30%, and for pure fluid. Both normalized torques increase with the gap Reynolds number. The normalized torque for the mixture is higher than the normalized torque for pure liquid. If the dependance of the normalized torque with Reynolds number is due to the suspending liquid inertial effects, the effect of the presence of particles would be to only increase the viscosity of the mixture. To account for the increase in flow viscosity due to the presence of particles, an effective gap Reynolds number ($Re_{b,\,eff}$) is considered. In this modified Reynolds number, the

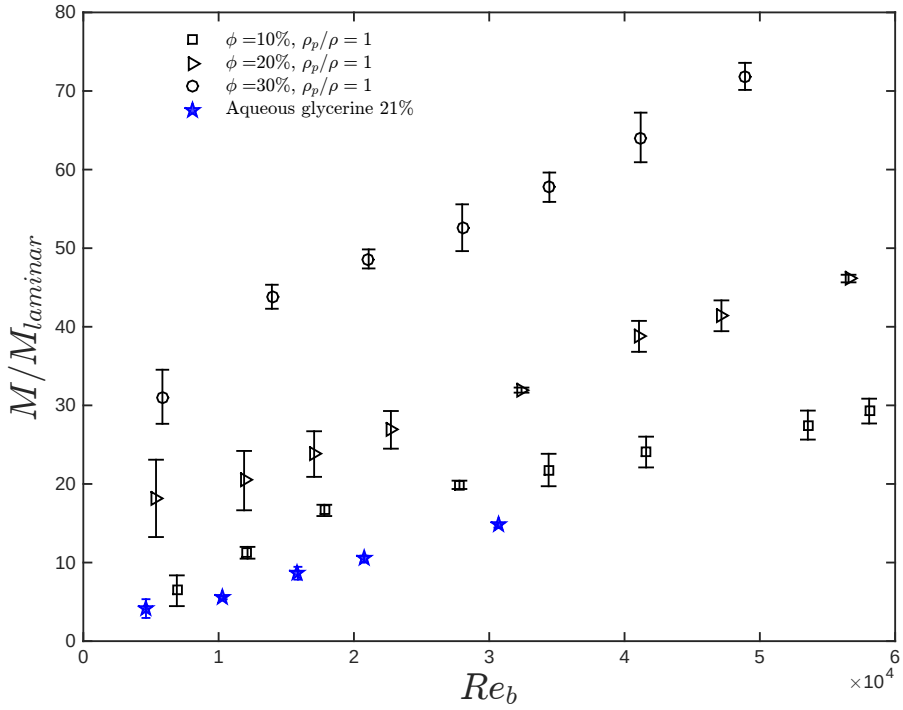


Figure 7.1: Normalized measured torques as a function of gap Reynolds numbers defined in equation 2.5 for pure fluid and mixtures with $\phi = 10$, 20 and 30% and $\rho_p/\rho = 1$.

effective viscosity of the mixture is used instead of the suspending liquid viscosity,

$$Re_{b,\,eff} = \frac{\rho \omega r_o b}{\mu'}.$$

The next step is to determine the effective viscosity of the mixture. Under no hydrodynamic effects, this effective viscosity would be independent of the Reynolds number and be only a function of volume fraction. Figure 7.2 shows the normalized torques for the experiments with $\rho_p/\rho = 1$ as a function of the loading fraction from the rough walls experiments of Koos et al. (2012) and the current experiments. For volume fractions lower than 40%, the data for the lowest Stokes numbers tested appear to coincide with the data from Koos (2012). As mentioned in Chapter 3, the range of Stokes numbers tested by Koos is slightly lower than the present experiments with $\rho_p/\rho = 1$ (Stokes number from $3 \leq St \leq 90$). Therefore, it is likely that hydrodynamics effects on the lowest Stokes numbers are negligible and the effective viscosity of the mixture can be inferred from these low St measurements. Figure 7.3 shows the effective relative viscosity of the mixture for the lowest Stokes numbers ($\mu'_{min}/\mu$) as a function of volume fraction compared with the effective relative viscosity from Koos et al. (2012). This effective viscosity is used to define the effective gap Reynolds number and it is considered to be only a function of volume fraction. To study the contribution from the hydrodynamic effects on the measured torques, it is instructive to normalize them by an "effective

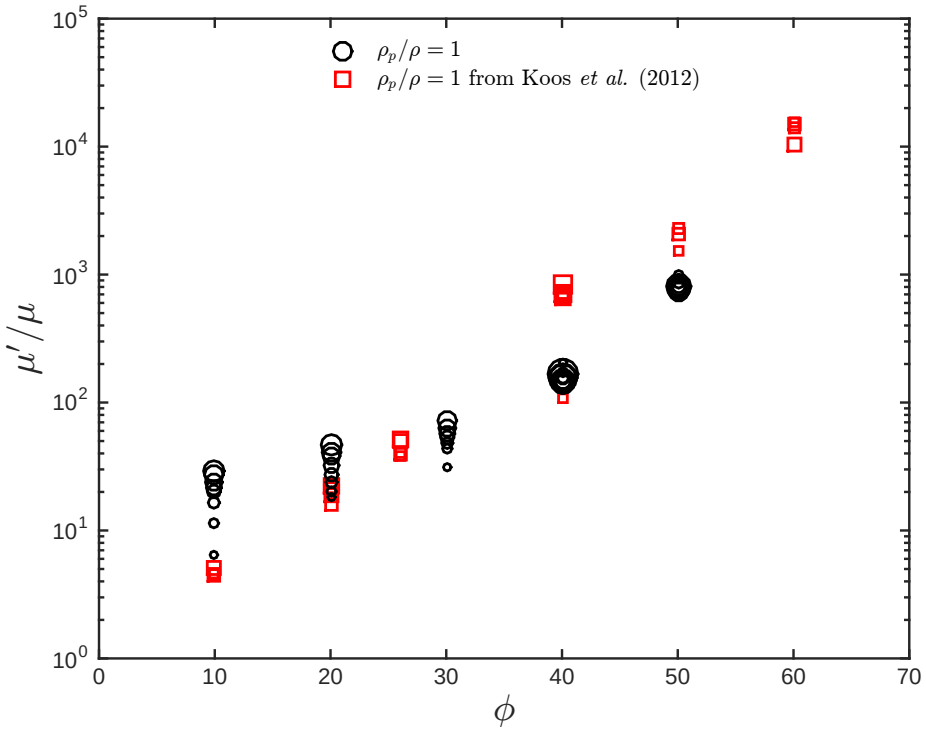


Figure 7.2: Effective relative viscosity as function of $\phi$ for current and previous work of Koos et al. (2012) with $\rho_p/\rho = 1$.

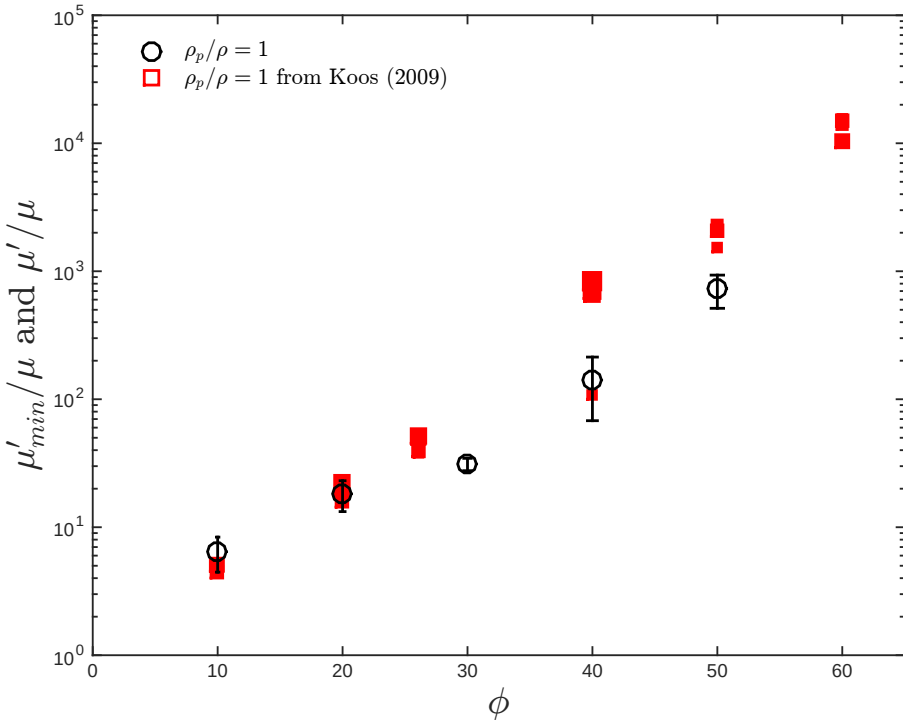


Figure 7.3: Minimum effective relative viscosity as function of $\phi$ for current experiments ($\mu'_{min}/\mu$) compared with the effective relative viscosity from Koos et al. (2012) with $\rho_p/\rho = 1$.

laminar torque", which is defined as a the corresponding torque for a Newtonian liquid with a viscosity equal to $\mu'_{min}(\phi)$,

$$M_{eff,\,laminar} = 2\pi r_i^2 H \dot{\gamma} \mu'_{min}(\phi).$$

If the effect of the presence of particles is to only increase the effective viscosity of the flow, the ratio between the measured torques and $M_{eff,\,laminar}$ would be independent of the effective gap Reynolds number when $Re_{b,\,eff}$ is below a critical value or regime, where the hydrodynamic effects are negligible.

Figure 7.4 shows the ratio between the measured torques and the effective laminar torque for all the volume fractions tested as a function of the effective gap Reynolds number based on $\mu'_{min}$. The range of effective gap Reynolds number goes from $1 \leq Re_{b,\,eff} \leq 10 \times 10^4$. If the results of Taylor (1936a) can be applied to the liquid-solid mixture, the critical Reynolds number for the onset of Taylor-Couette vortices is expected to occur about $Re_{b,\,eff} \approx 1.1 \times 10^4$ for the current geometry of the apparatus. From Figure 7.4 it can be seen that the normalized torque increases for effective Reynolds numbers in a lower range. However, pure fluid torque measurements showed that the measured torques deviate from the laminar theory at a similar gap Reynolds number range (see Figure 2.13). Figure 7.5 shows the pure fluid and mixture measurements as a function of

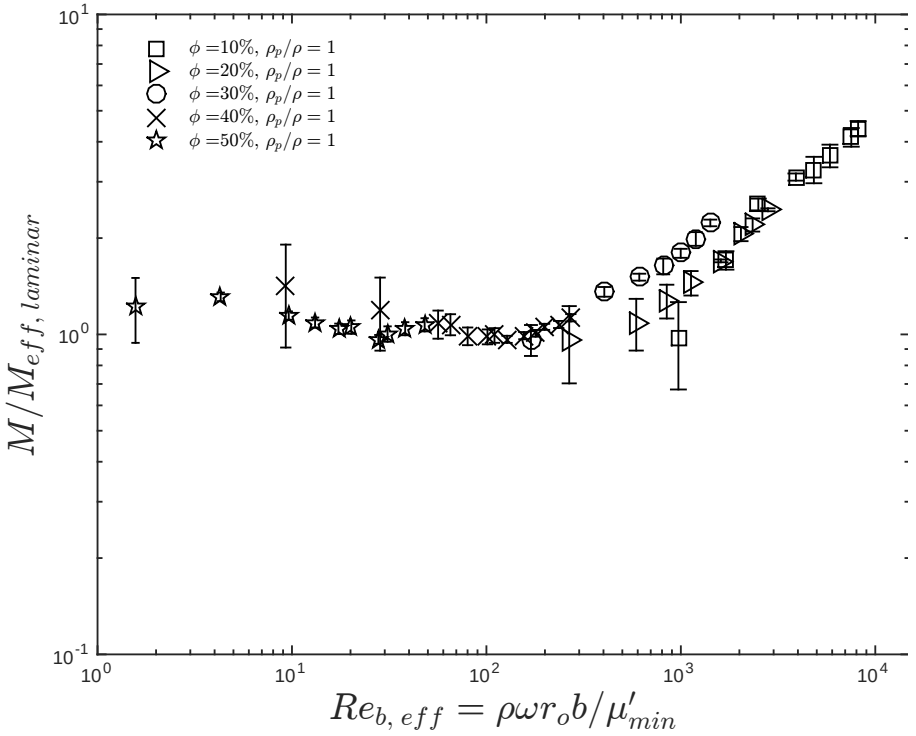


Figure 7.4: Measure toques normalized by effective laminar torque as a function of effective Reynolds number defined by the minimum value of $\mu'/\mu$ for each volume fraction.

gap and effective gap Reynolds number. The deviation from laminar theory occurs at an effective

Reynolds number range where the pure fluid measurements exhibit a non-laminar behavior. The mixture normalized torques start deviating from the laminar theory at lower effective Reynolds number range. In the Couette-Taylor flow studies from Taylor (1936a), it was shown that when the flow is sheared by the rotation of the outer cylinder, the flow transition did not occur at a specific critical gap Reynolds number but within a range. Based on this, it is likely that the hydrodynamic effects are present in a range of Reynolds number rather than above a critical value. Therefore, the deviation from the laminar behavior of the mixture at effective gap Reynolds number is more likely to be due to hydrodynamics effects rather than an effect of particle interactions.

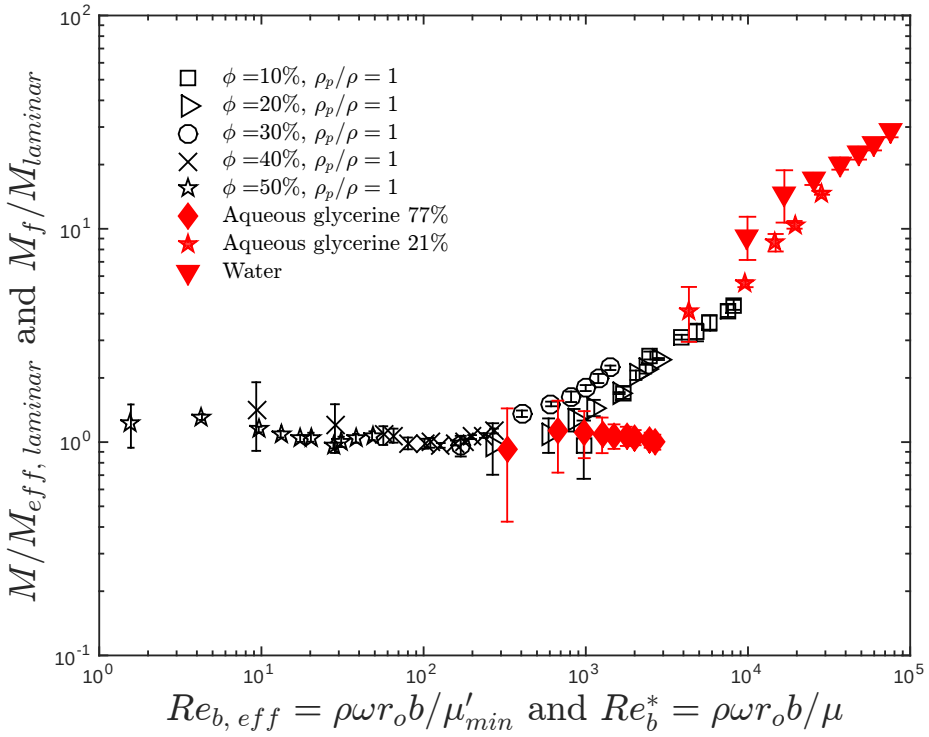


Figure 7.5: Measure toques normalized by $M_{eff,\,laminar}$ as a function of $Re_{b,\,eff}$ compared with normalized pure fluid torque measurements. For pure fluid, the normalized torques are plotted against $Re_b^*$.

In an ideal scenario where secondary flow effects are not present, the transition from "viscous" to "inertial" regime in liquid-solid flows would be governed by particle interactions. These interactions are controlled by the Stokes number, which is based on the particle size and the fluid viscosity rather than the effective viscosity of the mixture. Therefore, it is not possible to determine what the Stokes number regime at which the transition occurs due to merely particle inertia is.

For larger volume fractions the relative effective viscosity exhibited a weaker dependance on the Stokes number (see Figure 4.4), suggesting that for these experiments the inertial effects from the fluid and particles are not present. From Figure 7.5 it can be seen that for $\phi = 40$ and 50%, the corresponding $Re_{b,\,eff}$ is lower and possibly below the critical Reynolds number.

## 7.2 Direct comparisons between $\rho_p/\rho = 1$ and $\rho_p/\rho = 1.05$

Figure 7.6 shows the ratio of torques as a function of the Stokes number for the lowest loading fraction (10%) for the case with settling and non settling particles. Above Stokes number higher than 60, the normalized torques for both cases seem to match . Visualizations of the flow (a detailed analysis of this is presented in Chapter 6) for the case of settling particles at $\bar{\phi} = 10\%$ show that for Stokes numbers lower than 60, the height of the column of particles is lower than the bottom fixed guard height. Therefore, for $St < 60$ the particles do not reach the test cylinder. For this reason the torque measurements for these shear rates are not considered.

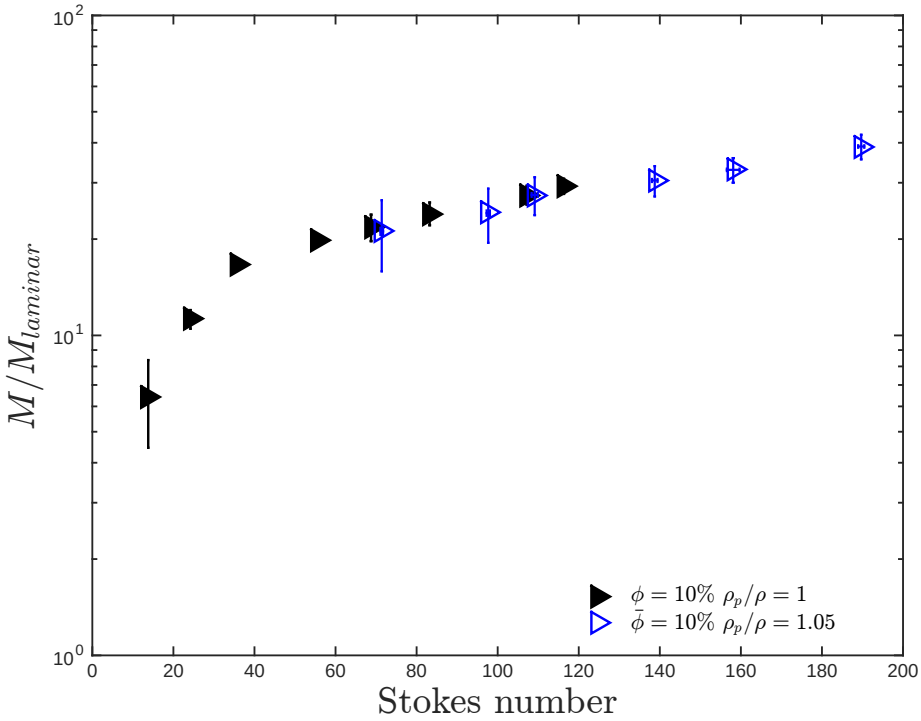


Figure 7.6: Normalized torques for 10% loading fractions as a function of St for $\rho_p/\rho = 1$ and 1.05.

Figure 7.7 shows the comparison between the normalized torques for a loading fraction of 10% with settling particles and the normalized torque measurements for just the liquid (plain water with no particles). These torques were normalized with the torque corresponding to a laminar flow. The normalized torques for a loading fraction of 10 % match the values for the torque measurements for just the fluid when the gap Reynolds number is lower than $5 \times 10^4$. For higher $Re_b$, the mixture exhibit higher normalized torques than the pure fluid. Above $Re = 3 \times 10^4$, the visualization of the flow starts showing the presence of particles in the middle test section.

The reason why the normalized torques for non-settling particles matches the normalized torques for the settling ones at $St < 135$ might be coincidental. In the case with settling particles, below

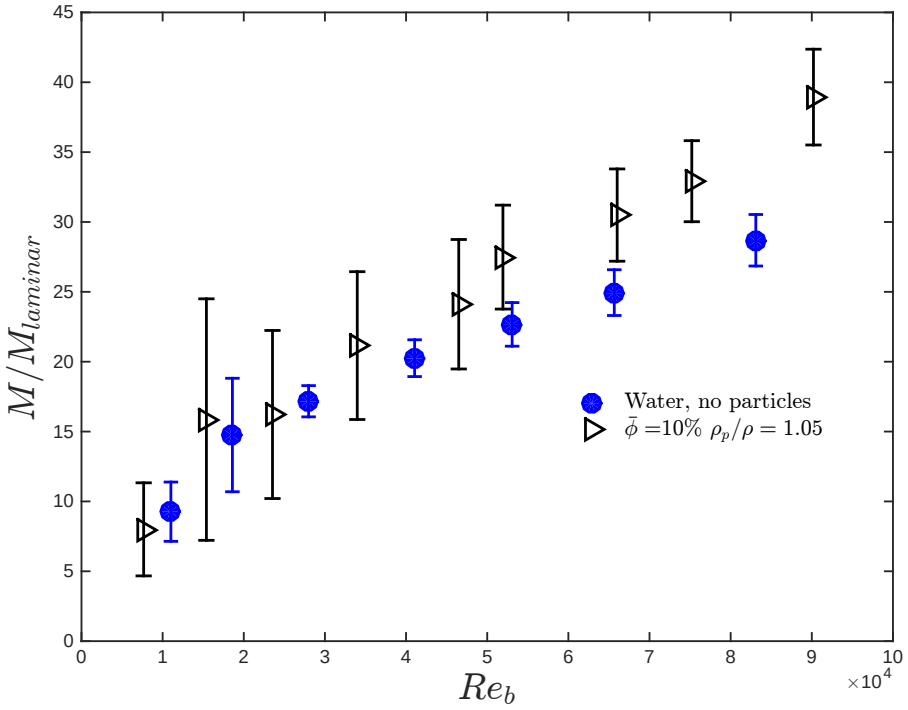


Figure 7.7: Comparison between normalized torques as a function of gap Reynolds number for pure fluid and $\bar{\phi} = 10\%$ with $\rho_p/\rho = 1.05$.

$St = 80$, the solid phase contribution to the torque at low shear rates is null, while for the case with neutrally buoyant particles the solid phase is always present (see Figure 7.8 for a comparison on the flow visualization between these two cases). Therefore at about $St = 80$, the measured torque includes a contribution from the pure fluid and a contribution from the particles.

For a higher loading fraction of 20%, the normalized torques for $\rho_p/\rho = 1$ are higher than for the case with $\rho_p/\rho = 1.05$ for $St > 60$, as seen in Figure 7.9. For the particular case of these low loading fractions, it is possible that the torque contribution from the suspending liquid is higher than the torque predicted from laminar theory. As presented in Section 2.4, the measured torques for plain water and 21% aqueous glycerine mixture are 4 to 28 times higher than the torques predicted by laminar theory. For the case of $\rho_p/\rho = 1.05$ and $\bar{\phi} = 10\%$, the visualization of the flow shows that the test cylinder is fully covered by the particles only for $St > 135$ (see Figure 6.14 or table 7.1). This means that for lower Stokes numbers, the measured torque does not correspond solely to the liquid-solid mixture and thus it is not representative of the suspension. A comparison of these loading fractions is given later in Section 7.6.

Figure 7.10 shows the normalized torques for a loading fraction of 30% for the case with settling and non-settling particles. For the case with settling particles, only the normalized torques corresponding to Stokes numbers where the particles are closed to be completely fluidized are considered (based on the settling particles heights and visualizations) so the settling effect on the measured

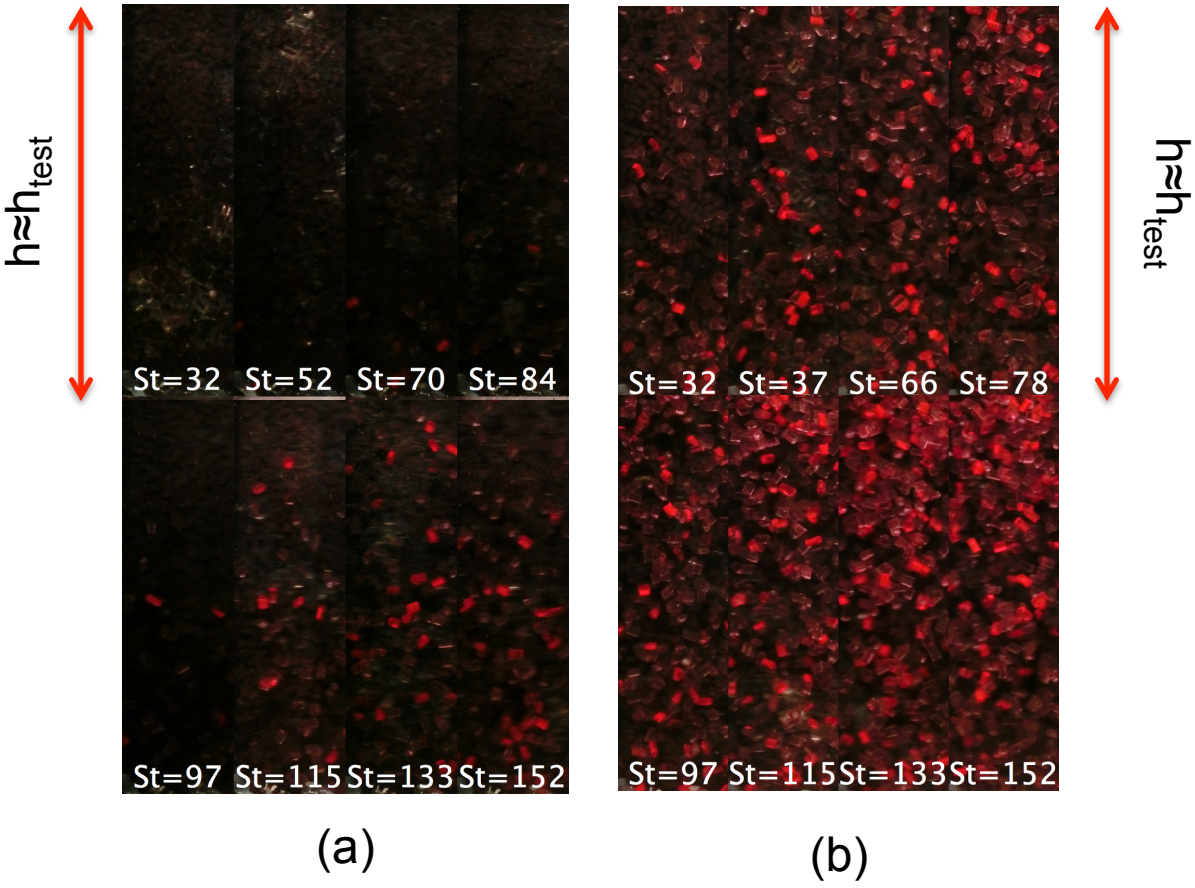


Figure 7.8: (a) Image sequence of the flow for $\bar{\phi} = 10\%$ and $\rho_p/\rho = 1.05$ for different Stokes numbers. (b) Same as (a) but for $\rho_p/\rho = 1$. The height of the visualization window is slightly higher than the test section.

| | No porous medium | | Porous medium | |
|---|---|---|---|---|
| $\bar{\phi}$ | St fully covered | St fluidized | St fully covered | St fluidized |
| 10 | 135 | NA | 80 | 80 |
| 20 | 80 | NA | 65 | 100 |
| 30 | NA | 80 | NA | 120 |
| 40 | NA | 95 | NA | 140 |
| 50 | NA | 100 | NA | 180 |
| 60 | NA | 100 | NA | NA |

Table 7.1: Critical Stokes numbers for fluidization. *St fully covered* denotes the Stokes number above which the test cylinder is fully covered by particles based on Figure 6.19. *St fluidized* denotes the Stokes number above which the ratio of torques exhibits a change in slope based on Figures 4.16 and 5.15.

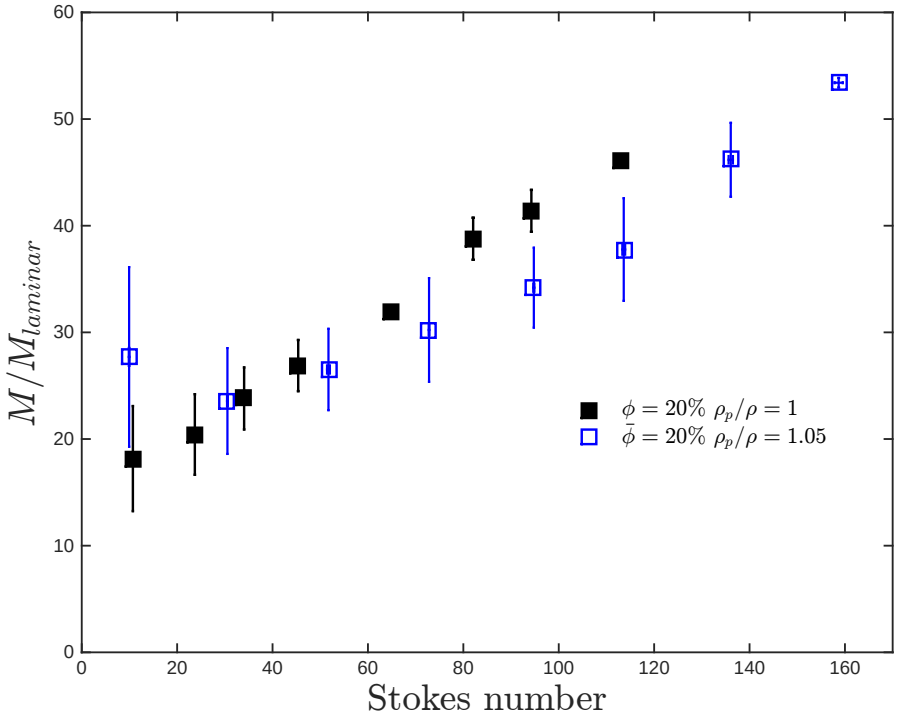


Figure 7.9: Comparison between normalized torques as a function of Stokes numbers for $\rho_p/\rho = 1$ and $\rho_p/\rho = 1.05$ with $\bar{\phi} = 20\%$.

torques is weaker. For both cases, the normalized torques increase with Stokes number and exhibit a linear dependance with similar slopes. The normalized torques for the settling particles at the two similar Stokes numbers are higher than for the non settling ones. A possible explanation for these differences is that the effective volume fraction for the settling particles is slightly higher. The Stokes number at which the particles reach the top of the rheometer (see table 7.1) is around 113, but even when the particles have reached the top, it does not imply an homogeneous distribution of the particles. A gradient on the volume fraction may exist, leading to effective volume fractions higher than the loading fractions and therefore higher normalized torques. An analysis of the effective volume fraction is presented in Section 7.3.

Based on the particles height measurements, the test cylinder is fully covered at most Stokes numbers for a loading fraction higher than 30% (see Figure 6.14 or table 7.1). The torque contribution from the suspending liquid might be less than in the more dilute cases since the concentration of particles is high enough to decrease the effective Reynolds number of the flow, making the suspending liquid contributions closer to the torque predicted from laminar theory. Figure 7.11 shows the normalized torques for the higher loading fractions and for $\rho_p/\rho = 1$ and $\rho_p/\rho = 1.05$ . Only the Stokes numbers at which the particles reached the top are considered. Predictions of the effective volume fraction based on the flow visualizations are presented later in Section 7.3. For the case with matched densities, there is a slight decrease in the effective relative viscosity for $\phi = 40$ and 50%

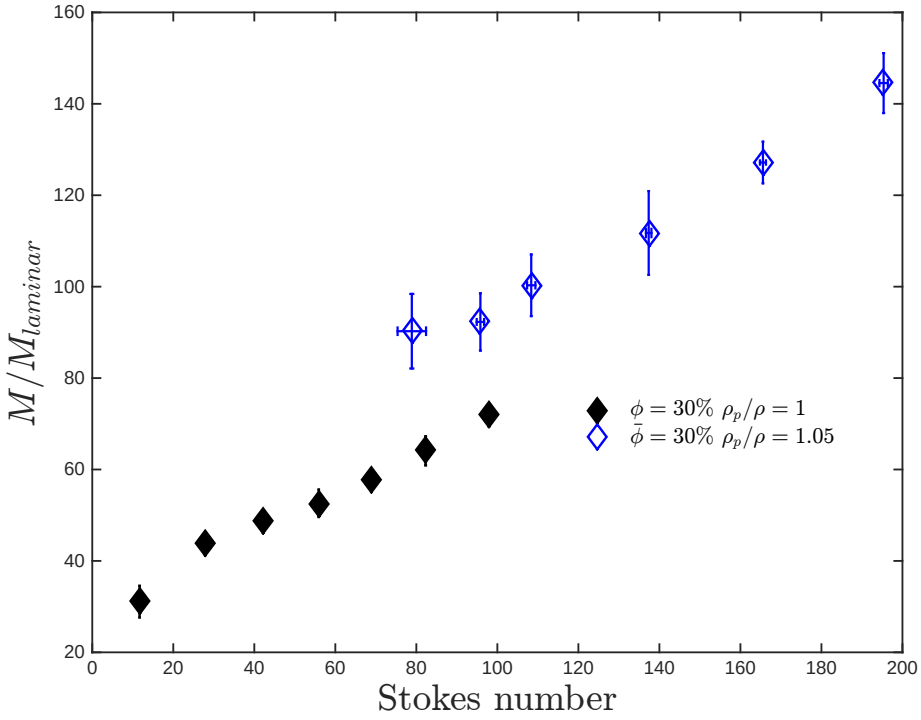


Figure 7.10: Comparison between normalized torques for $\rho_p/\rho = 1$ and $\rho_p/\rho = 1.05$ as a function of Stokes numbers with $\bar{\phi} = 30\%$. For the case of $\rho_p/\rho = 1.05$, only the data without settling is shown.

at the lowest Stokes number, and this decrease might be due to slight settling of the particles, but it is considerably less dramatic than the one observed for settling particles at low Stokes numbers (see Figure 4.15). The normalized torques for $\phi = 50\%$ for $\rho_p/\rho = 1$ are almost the same as for $\rho_p/\rho = 1.05$. At this high loading fraction the effective volume fraction after fluidization matches the effective volume fraction for $\rho_p/\rho = 1$. For $\phi = 40\%$ and $\rho_p/\rho = 1$ the normalized torques have lower values than for $\rho_p/\rho = 1.05$, and it is possible that there exists differences in effective volume fraction due to settling.

For all the cases shown in Figure 7.11, the normalized torques exhibit a weak dependance on the Stokes number. In the absent of strong hydrodynamics effects, the normalized torques would depend on the concentration and possible interaction of particles. If the latter is not present or if it is weak, the normalized torques would be independent of Stokes number and would exhibit a strong dependance on volume fraction. Therefore, for these loading fractions, the effects of fluid and particle inertia are not strong. An analysis of the inertial effects for the case with $\rho_p/\rho = 1.05$ is presented in Section 7.4.

The normalized torques for Stokes numbers where the particles are completely fluidized and for loading fractions higher than 20% seem to coincide with the normalized torques for the case with $\rho_p/\rho = 1$ as can be observed in Figure 7.12.

Assuming that the normalized torques are equal to the effective relative viscosity, Figure 7.13

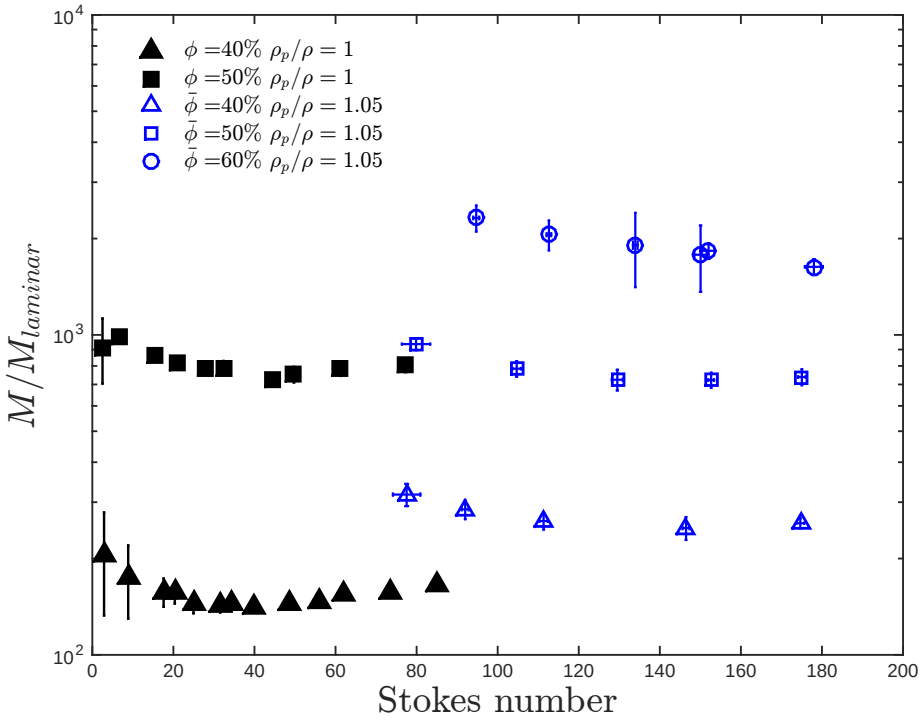


Figure 7.11: Normalized torques as a function of Stokes numbers with $\bar{\phi} = 40$, 50, and 60% for $\rho_p/\rho = 1$ and $\rho_p/\rho = 1.05$. For the case of $\rho_p/\rho = 1.05$, only the data without settling is shown.

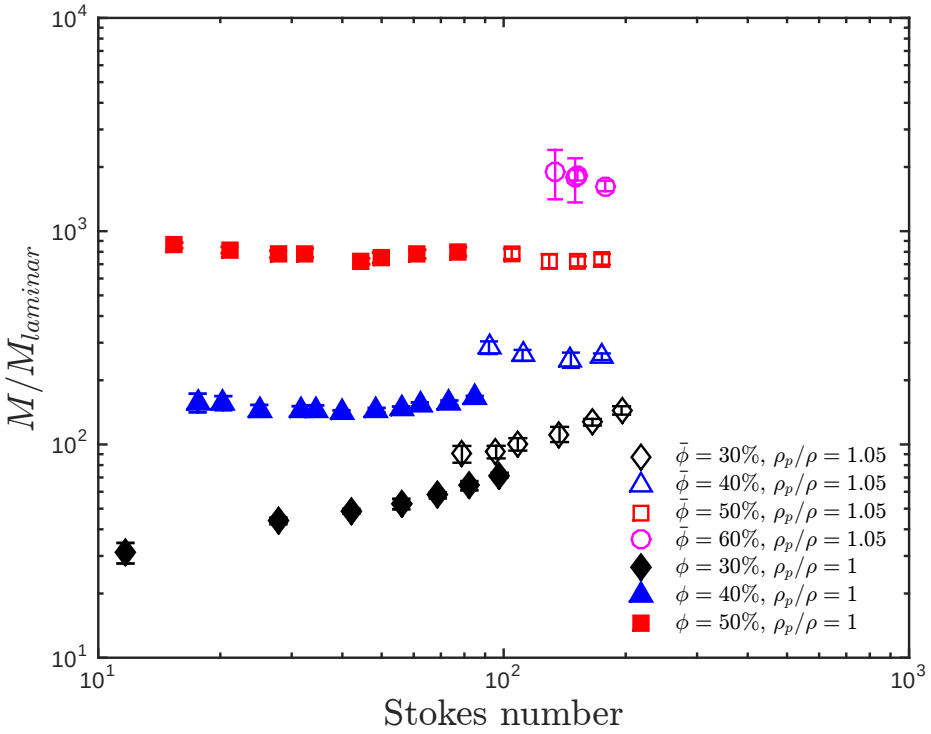


Figure 7.12: Normalized torques as a function of Stokes number for $\rho_p/\rho = 1$ and $\rho_p/\rho = 1.05$. For the case with settling particles, only the normalized torques corresponding to Stokes number where the particles are fully fluidized are shown.

shows the effective relative viscosity for all the volume fraction tested and for $\rho_p/\rho = 1$ and $\rho_p/\rho = 1.05$. For the case with settling particles, the data corresponding to Stokes numbers below the fluidization threshold are not included. The Stokes number magnitude is denoted by the size of the symbol. The effect of Stokes number is the same for both density ratios. For loading fractions lower than 40%, the effective relative viscosity increases with St. At higher loading fractions the effect of Stokes is not very noticeable for the both density ratios studied as long as the data with settling effects are not considered. Figure 7.14 shows the ratio of $\mu'/\mu$ for all the Stokes number tested, including the data where the particles are settling. It can be seen from Figure 7.14 that for loading fractions higher than 20%, the ratio of $\mu'/\mu$ decreases with St for $\rho_p/\rho = 1.05$. This is linked to the settling effects and it is similar to what was observed by Acrivos et al. (1994). It is expected that these two curves would collapse when the effective volume fraction is used instead of the loading fraction. The prediction of the effective volume fraction is studied in the next section.

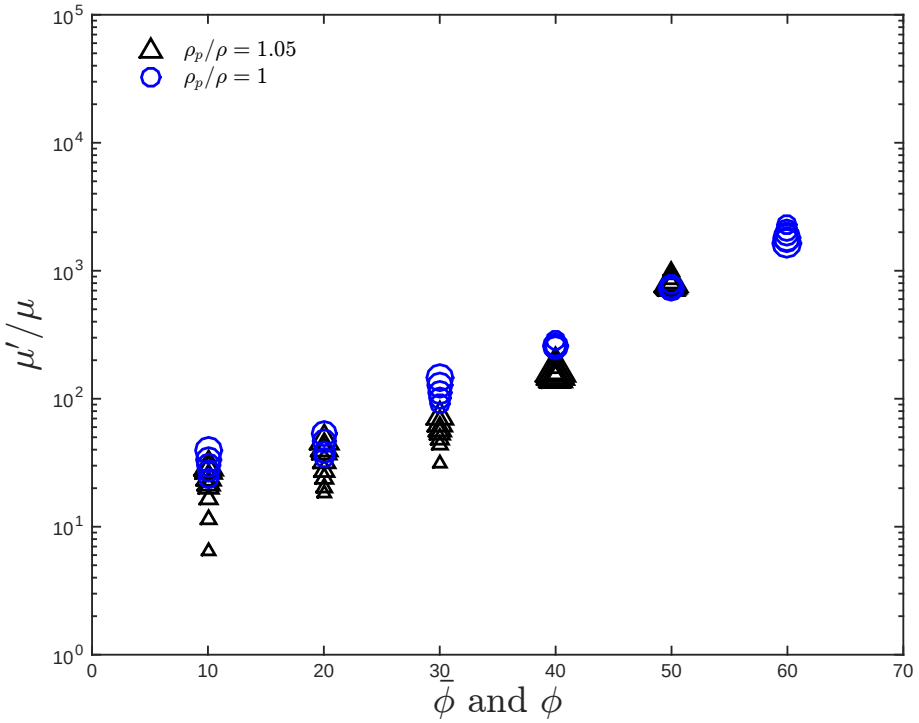


Figure 7.13: Relative effective viscosity as a function of $\phi$ and $\bar{\phi}$ for $\rho_p/\rho = 1$ and $\rho_p/\rho = 1.05$. For the case of $\rho_p/\rho = 1.05$, only the data without settling is shown.

A comparison between the two sets of data for the current experiments and the rough walls experiments from Koos et al. (2012) is presented in Figure 7.15.

The effect of Stokes number is considerably less for the previous experiments of Koos (2009) at lower volume fractions.

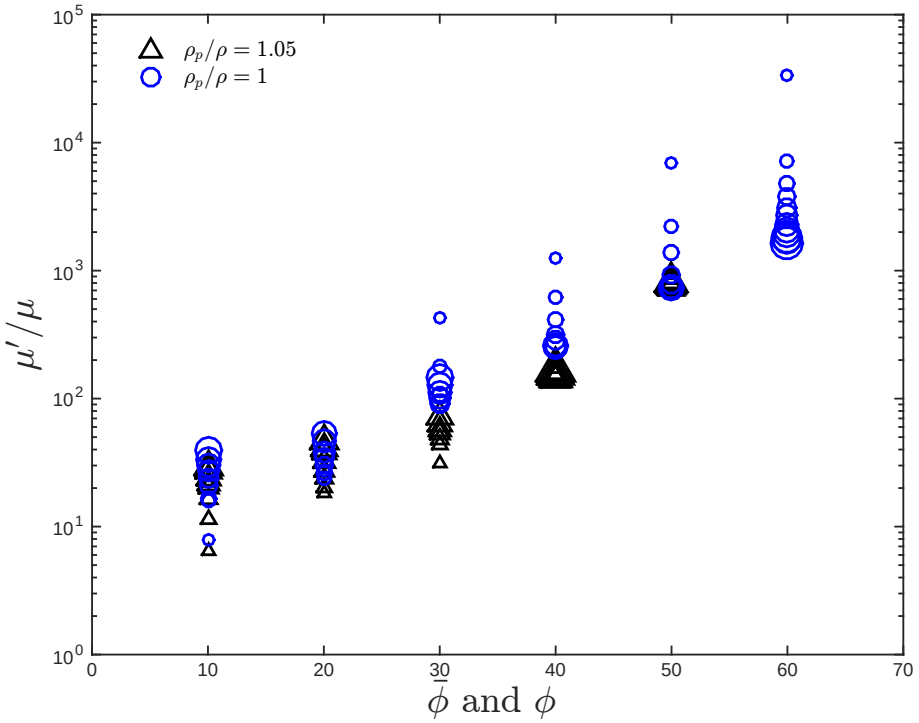


Figure 7.14: Relative effective viscosity as a function of $\phi$ and $\bar{\phi}$ for $\rho_p/\rho = 1$ and $\rho_p/\rho = 1.05$. All the Stokes number tested are shown, including the ones with settling effects.

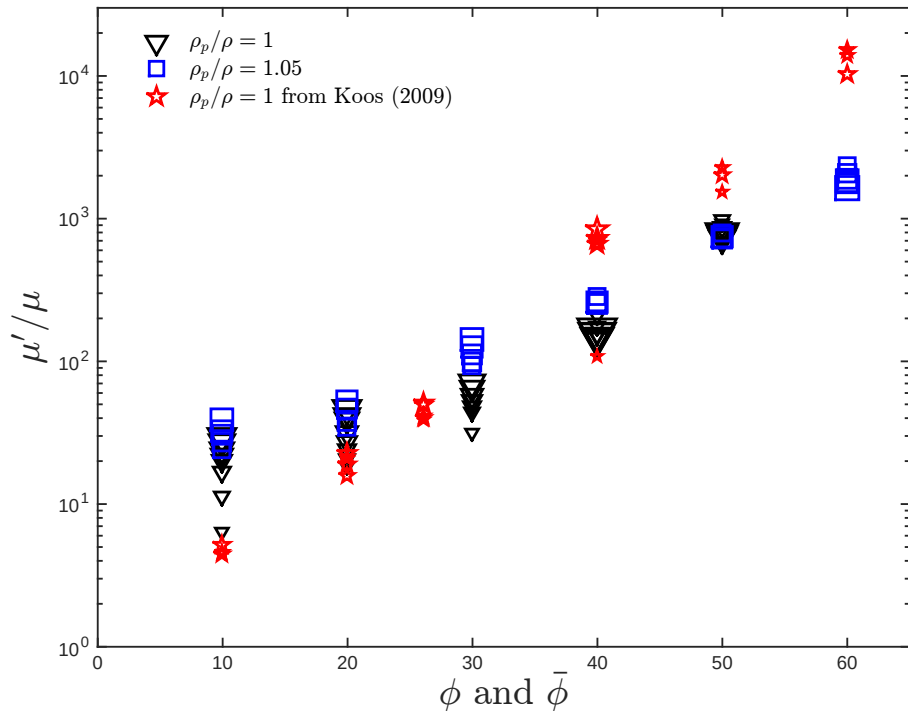


Figure 7.15: Relative effective viscosity as a function of $\phi$ and $\bar{\phi}$ for $\rho_p/\rho = 1$ and $\rho_p/\rho = 1.05$ compared with the effective relative viscosity from Koos et al. (2012). For the case of $\rho_p/\rho = 1.05$, only the data without settling is shown.

## 7.3 Prediction of the effective volume fraction

As mentioned before in Section 7.2, for settling particles at low loading fractions and below a certain Stokes number, the particles do not entirely cover the test cylinder. To compare these low loading fractions and the low loading fractions with $\rho_p/\rho = 1$, only the measurements where the test cylinder is fully covered are considered.

Figure 7.16 shows the effective relative viscosity as a function of the Stokes numbers for $\phi = 10$ and 20%, and for $\rho_p/\rho = 1$ and $\rho_p/\rho = 1.05$. For the lowest volume fraction the effective relative viscosity for the settling particles appears to coincide with the trend observed for $\rho_p/\rho = 1$. However, the St numbers at which the particles fully covered the test cylinder are higher than the tested St for $\rho_p/\rho = 1$ but they seem to follow the same trend. This suggests that the difference in density is less important when the particles are completely fluidized for this dilute case.

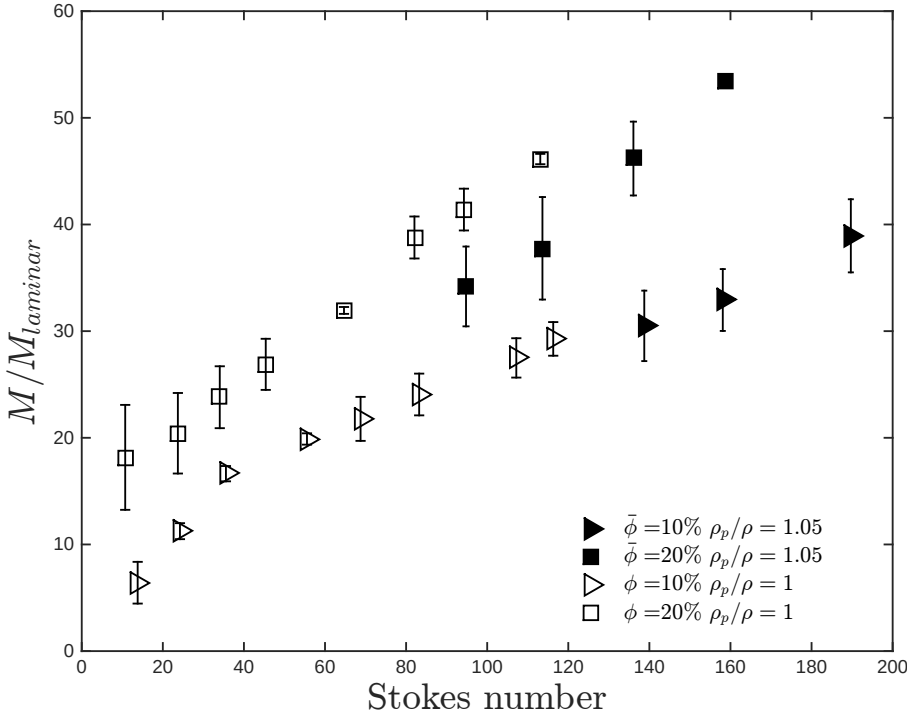


Figure 7.16: Relative effective viscosity as a function of Stokes numbers with $\bar{\phi} = 10$ and 20% for $\rho_p/\rho = 1$ and $\rho_p/\rho = 1.05$. For the case of $\rho_p/\rho = 1.05$, only the data without settling is shown.

For the higher loading fraction of 20%, the effective relative viscosity for the settling particles is slightly lower than for the density matched experiments with same loading fraction. This difference is an indication of the particles' effect since the suspending liquid for the case with settling particles has a lower viscosity than for the case with $\rho_p/\rho = 1$. Thus, an increase in the effective relative viscosity must be due to an increase in the particle concentration. In Figure 7.17, visualization of the flow is shown for a loading fraction of 20%, where it can be seen in the difference in particle

concentration.

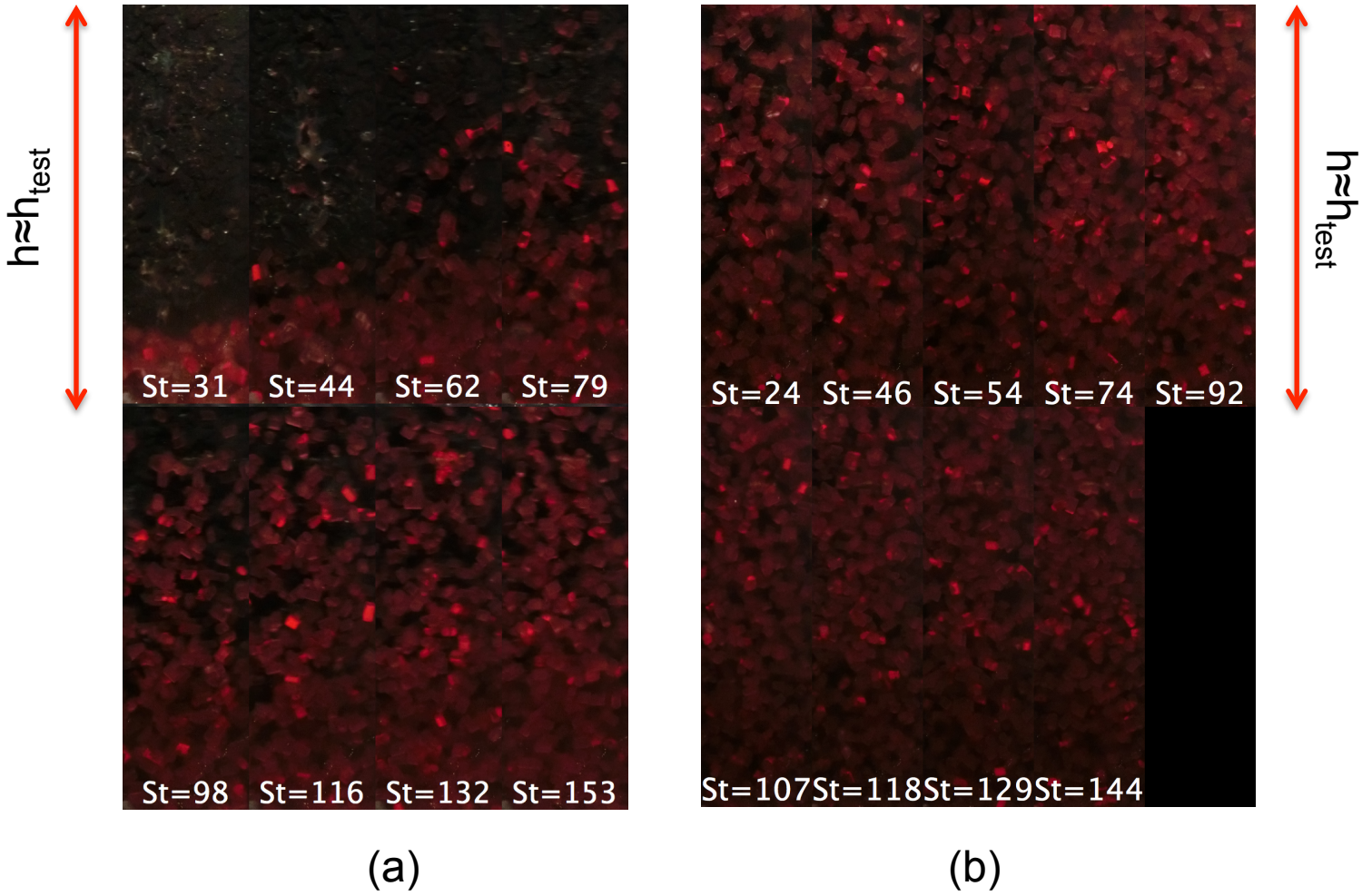


Figure 7.17: (a) Image sequence of the flow for $\bar{\phi} = 20\%$ and $\rho_p/\rho = 1.05$ for different Stokes numbers. (b) Same as (a) but for $\rho_p/\rho = 1$. The height of the visualization window is slightly higher than the test cylinder.

To account for the effect of solid concentration, the effective volume fraction for the settling particles is inferred from the particle resuspension measurements. Using a linear interpolation, the effective volume fraction at specific query Stokes number can be inferred from the volume fraction calculated using the particles height measurements presented in Chapter 6. Figure 7.18 shows the effective relative viscosity as a function of the effective volume fraction for different Stokes numbers tested for $\rho_p/\rho = 1.05$. Here only the cases where the test cylinder is fully covered are considered. The magnitude of the Stokes numbers is represented with different size symbols (the larger the Stokes number, the larger the symbol). As the Stokes number increases, the effective volume fraction decreases. The highest relative viscosity corresponds to the highest volume fraction and the lowest

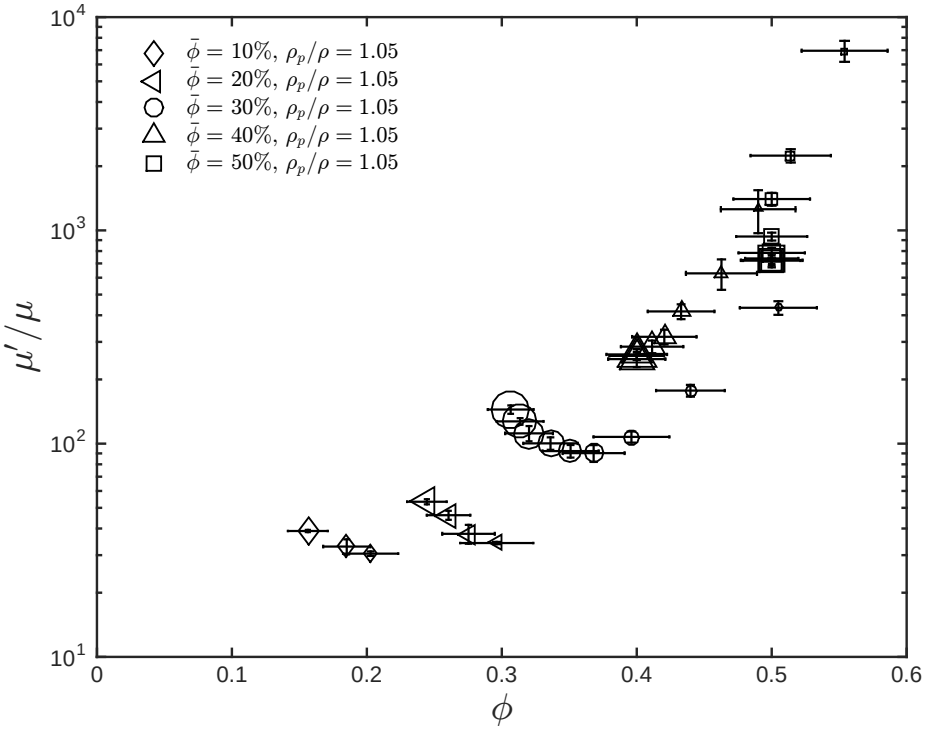


Figure 7.18: Effective relative viscosity as a function of the predicted volume fraction. The size of the symbols denotes the magnitude of the Stokes numbers, where the largest symbols correspond to the largest Stokes numbers. Only the cases where the mixture cover the test cylinder are presented.

Stokes number. For loading fractions higher than 30%, the data seem to collapse. For the cases with lower $\bar{\phi}$, the data seem to scatter more.

To study the effect on differences in density, the effective relative viscosity and volume fraction are compared with the case with $\rho_p/\rho = 1.$ . Figure 7.19 shows this comparison.

The effective relative viscosity for the two sets of data seems to coincide and follow the same trend. This suggests that there are no strong effects on different density ratios. Figure 7.20 shows the comparison between the current experiments and the previous experiments from Koos (2009).

The data seem to coincide for most volume fractions. The loading fractions that deviate more are the loading fraction of 10 and 40% from Koos (2009).

## 7.4 Inertial and particle concentration effects on mixtures with $\rho_p/\rho = 1$

The predicted effective volume fraction is used to estimate the effective viscosity of the mixture. Based on Figure 7.3, the effective viscosity of the mixture for a $\rho_p/\rho = 1.5$ is assumed to be independent of the density ratio. This assumption is validated with the results presented in the previous section, where the effect of differences in density was weak (it should be noted that the

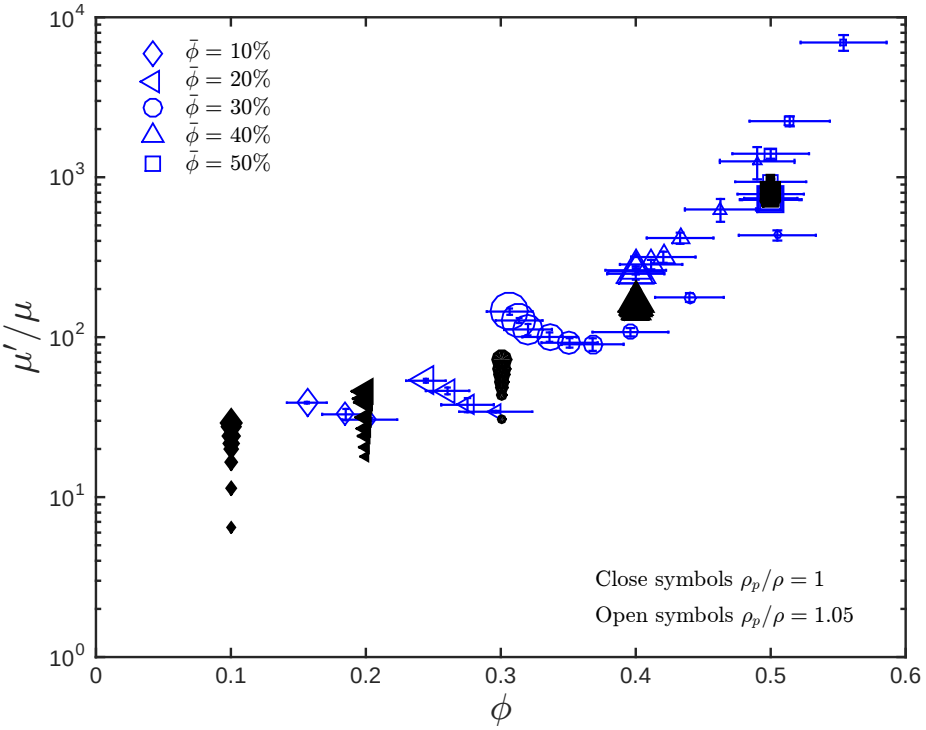


Figure 7.19: Effective relative viscosity as a function of the loading and predicted volume fraction for $\rho_p/\rho = 1$ and $\rho_p/\rho = 1.05$.The size of the symbols denotes the magnitude of the Stokes numbers, where the largest symbols correspond to the largest Stokes numbers. Only the cases where the mixture cover the test cylinder are presented.

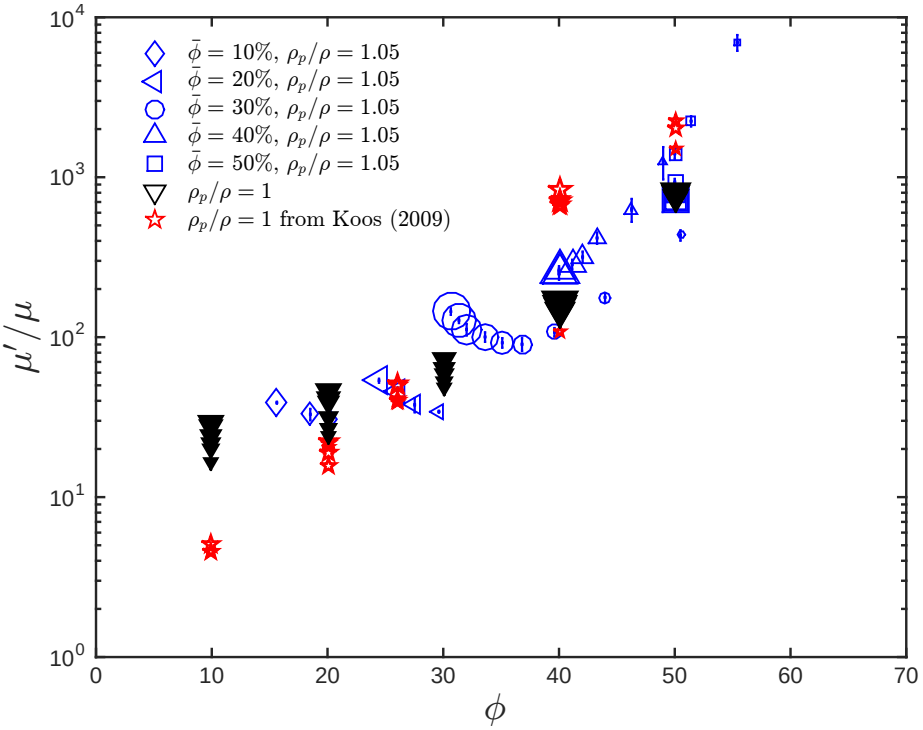


Figure 7.20: Effective relative viscosity as a function of the loading and predicted volume fraction for $\rho_p/\rho = 1$ and $\rho_p/\rho = 1.05$, compared with the data from rough walls of Koos (2012). The size of the symbols denotes the magnitude of the Stokes numbers, where the largest symbols correspond to the largest Stokes numbers. Only the cases where the mixture cover the test cylinder are presented.

differences in density is only 5%). It follows then that the normalized torque corresponding to the same volume fraction would be the same as long as no hydrodynamics effects are present. Based on this, the effective relative viscosity between two mixtures with different suspending liquid but same volume fraction is

$$\frac{\mu'_{min,\ 21\%\ glycerine}}{\mu_{21\%\ glycerine}} = \frac{\mu'_{min,\ H_2O}}{\mu_{H_2O}}.$$

Using this relation the effective viscosity is found for the experiments with settling particles. The effective Reynolds number is calculated in the same way as before. Figure 7.21 shows the measured torques normalized with the corresponding laminar torque for a effective mixture viscosity. Only the data with fluidized particles is considered to isolate the effect of settling.

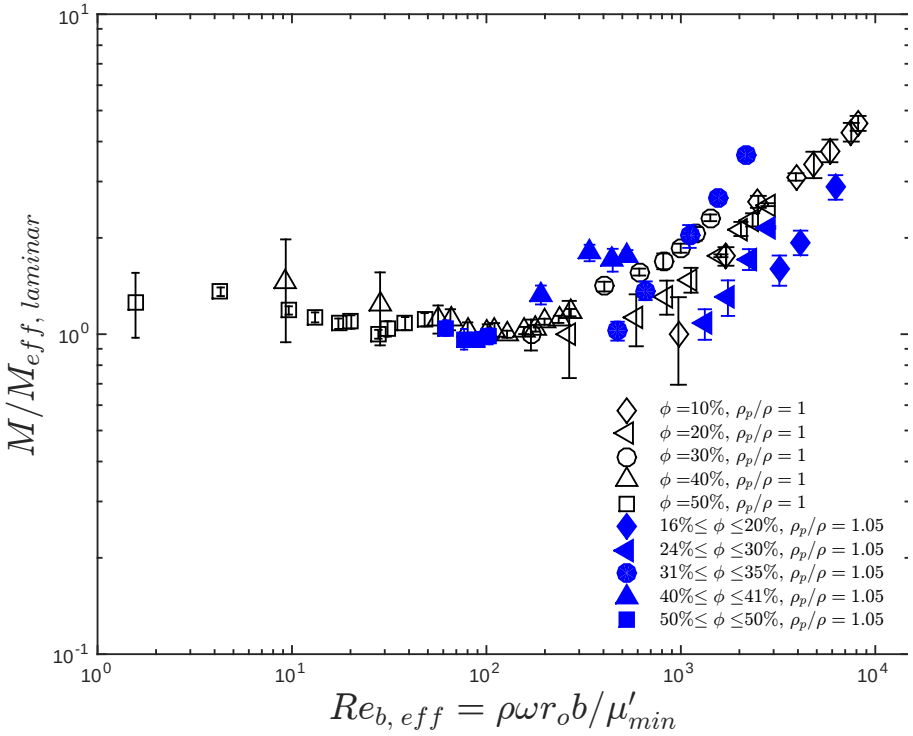


Figure 7.21: Measured torques normalized with effective laminar torque as a function of $Re_{b,\ eff}$ for $\rho_p/\rho = 1.05$. The effective viscosity of the mixture is inferred from the effective volume fraction and Figure 7.3.

The settling particles show a wider scatter than the data with density ratio equal to one. This is due to the uncertainties introduced when estimating the effective viscosity of the mixture ($\mu'_{min}$). The accumulative uncertainty would involve the uncertainty on predicting the effective volume fraction and the uncertainty involved inferring $\mu'_{min}$ from the data with $\rho_p/\rho = 1$. If the mixture effective viscosity is considered to be equal to the effective viscosity for the lowest values of Stokes number found for $\rho_p/\rho = 1.05$, then the source of uncertainties reduces. In such case the modified

effective Reynolds number is defined as

$$Re^*_{b,\,eff} = \frac{\rho\omega b}{\mu'^*_{min}},$$

where $\mu'^*_{min}$ corresponds to the minimum value of $\mu'/\mu$ found for each loading fraction. For the case with $\rho_p/\rho = 1.05$, this corresponds to the highest Stokes numbers where the particles are fully fluidized. Figure 7.22 shows the measured torques normalized by the effective laminar torque considering $\mu'^*_{min}$ ($M^*_{eff,\,laminar}$). The scattered in this plot is considerably less.

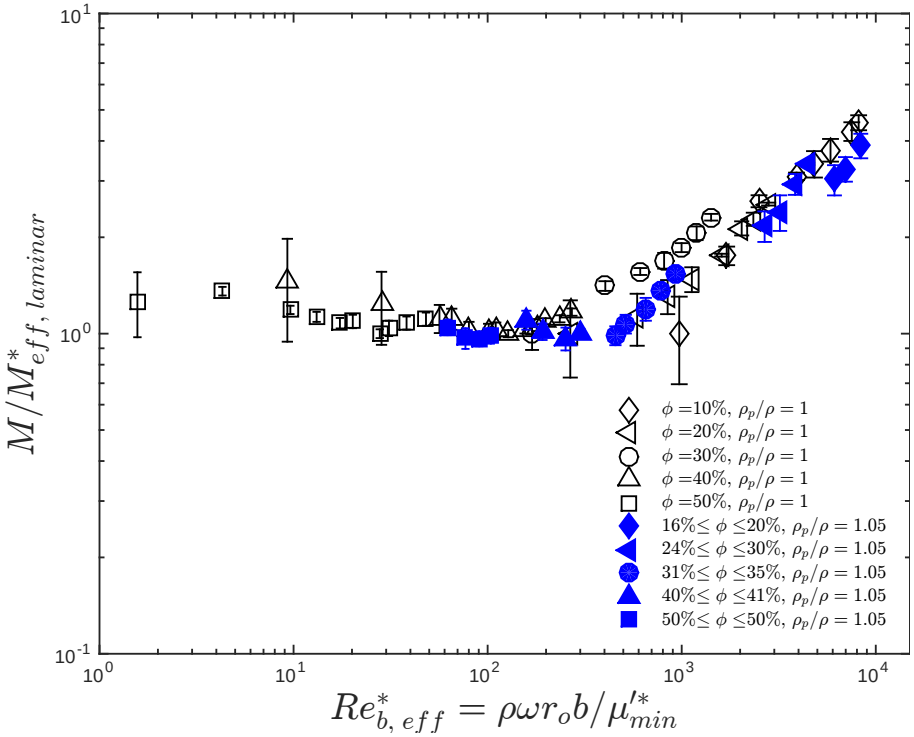


Figure 7.22: Measured torques normalized with effective laminar torque as a function of $Re^*_{b,\,eff}$ for $\rho_p/\rho = 1.05$. The effective viscosity of the mixture used for $Re^*_{b,\,eff}$ corresponds to the minimum $\mu'/\mu$ for each loading fraction.

In both figures the range of effective Reynolds number at which the normalized torques deviate from a laminar behavior coincides with the region found for the case with $\rho_p/\rho = 1$. Based on these results, any dependance of the Stokes or Reynolds number is due to hydrodynamics effects.

## 7.5 Flow over a porous medium $\rho_p/\rho = 1.05$

In an attempt to study low loading fractions, experiments of the mixture flow over a porous medium were performed. For all the loading fractions, the normalized torques decrease with Stokes numbers, with the exemption of $\bar{\phi} = 10\%$. One of the main differences found between these experiments and

the ones without a porous bed is that the measured torque decreases at a certain Stokes number. This is observed at all loading fractions and it was independent of the shearing history of the flow (no hysteresis). This drop on the measured torque is likely to be linked to a settling (or equivalently to a resuspension effect). This drop in torque is observed as a change in slope on the normalized torques. A comparison between the visualization of the flow and the relative viscosity is presented in the next section.

### Effect of resuspension on flow over a porous medium

Figure 7.23 (a) shows the flow visualization for a 10% loading fraction at different Stokes numbers. Each image was taken after several minutes of shearing the flow at a constant shear rate for each St. As mentioned in the previous chapter, the height of the visualization window for these experiments is approximately one inch higher than the test cylinder. Therefore, only the flow in this region, which is the same region where the torque measurements take place, is visualized. The corresponding St for each image increases from left to right, starting at the upper left corner with a $St = 0$. The height reached by the particles increases considerably when the St goes from 0 to 18 and it remains almost constant between St from 18 to 55 (see Figure 6.17 to see the actual height measurements). There is a bigger increase in height when the St goes from 67 to 81, and when $St = 109$ the particles appeared to be completely resuspended and covered the whole test cylinder. These observations can be compared with the effective relative viscosity measurements. In Figure 7.23 (b) it can be observed that $\mu'/\mu$ corresponding to the measurements that were taken from low to high shear rates (closed symbols), decreases abruptly when St increases from 10 to 34. This abrupt change in $\mu'/\mu$ coincides with the abrupt increase in the height reached by the particles between $0 \leq St \leq 18$. This means that the mixture requires higher shear stress in order to initiate the flow of settled particles, and as soon as the particles became re-suspended the needed shear stress decreased. For St larger than 20, $\mu'/\mu$ remains almost constant. When the $St$ is higher than 80, $\mu'/\mu$ starts increasing. As pointed out previously in Chapter 5, this increase was only observed for this particular loading fraction. It is possible that this behavior is due to settling effects. By simply comparing the top and bottom row of the image sequence in Figure 7.23 (a), the big difference between the area covered by particles for St lower than 91 (top row) and the area covered for St higher than 100 can be noticed. The ratio between the highest and the lowest normalized height for this loading fraction (see Figure 6.17) is 2.06, while the ratio for a loading fraction of 20% is 1.51. Even when the particles are more packed at low Stokes numbers, they don't cover a significant region of the area where the torque measurements are taken. When the particles fluidized, they are more diluted but they cover a bigger region of the test area. In the following section, an analysis about the possible hydrodynamics effects present in this set of experiments is presented. Because of the limitation of the short visualization window used for these experiments, measurements of the total height reached by the particles when

fluidized are not available. The ratio $\mu'/\mu$ keeps increasing for St higher than 120. It is possible that this increase on $\mu'/\mu$ is due to inertial effects.

When the experiments are performed from high to low shear rates (Figure 7.23 open symbols), and for St higher than 80; the effective relative viscosity exhibited the same behavior as for the case where the shear rate went from low to high. For St lower than 80, the $\mu'/\mu$ for high to low shear rate experiments is higher. These differences were only observed for this loading fraction and the reason why is not completely clear. The glass beads that formed the porous media and the settling polystyrene particles re-arranged themselves after being sheared at high shear rates, which increased the settling height of the particles and the effective volume fraction.

Figure 7.24 shows the visualization for flow over a porous media with a loading fraction of 20%. Similar to what is observed in Figure 7.23 (a), the height reached by the particles for Stokes numbers lower than 80 increases gradually but not abruptly. For $St = 82$ there is an abrupt increase in height and the particles covered the whole visualization window. As St increases, the images for the visualization look very similar to each other. In Figure 7.24 (b) the $\mu'/\mu$ as a function of St is presented. Unlike the case for a loading fraction of 10%, the effective relative viscosity decreased considerably for St lower than 82 (the ratio between the $\mu'/\mu$ for the lowest St and the minimum $\mu'/\mu$ for a loading fraction of 20% is 13, meanwhile for a 10% loading fraction that ratio is 2.9). For St higher than 82, $\mu'/\mu$ remains fairly constant. Since there was not a significant variation between the images corresponding to such St, the reason why $\mu'/\mu$ appears to be independent of the St could be that the effective volume fraction remained constant.

For the case with a 30% loading fraction presented in Figure 7.25 (a), the particles covered almost the entire visualization window. It can be seen that the particles start rising gradually for St lower than 74. Due to the visualization window size it is not possible to see if there was an abrupt change in the height reached by the particles. However, the $\mu'/\mu$ measurements (Figure 7.25 (b)) show a change in slope for St higher than 120. It is possible that the particles' full resuspension occurs at a higher St than for the lower loading fraction cases.

For larger loading fractions, the area where the torque measurements take place was completely covered by the particles, as shown in Figure 7.26. Based on these images it is not possible to identify when the particles are fully fluidized because of the size of the visualization window. However, as described in Chapter 5, the effective relative viscosity does exhibit a change in slope at Stokes numbers between 120 and 130 (see Figure 7.27). These findings suggest that the effective volume fraction became constant for St higher than 130.

## Direct comparisons between flow with and without a porous medium base

Figure 7.28 shows the normalized torques for loading fractions of 20% for the case with different density ratios for $\bar{\phi} = 10\%$ over a porous medium. For the case with settling particles, only the

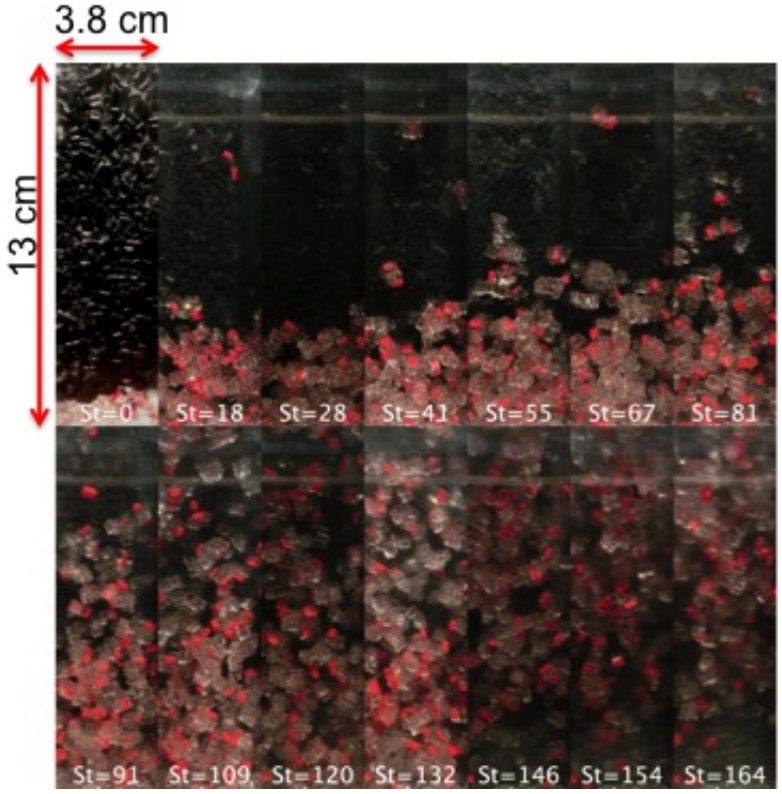


(a)

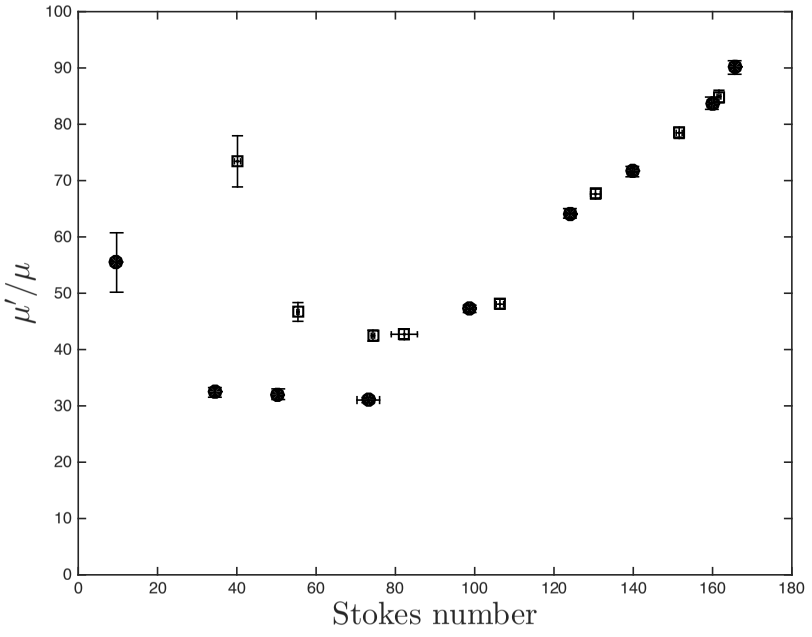


(b)

Figure 7.23: (a) Image sequence of flow over porous media with a loading fraction of 10% for different Stokes numbers. The height of the visualization window is the same as the height of the inner middle cylinder where the torque measurements are taken. (b) Effective relative viscosity as a function of Stokes number for loading fraction of 10% over a porous media. Closed symbols correspond to measurements taken with increasing shear rate. Open symbols correspond to measurements taken from high to low shear rates. $\rho_p/\rho = 1.03$.

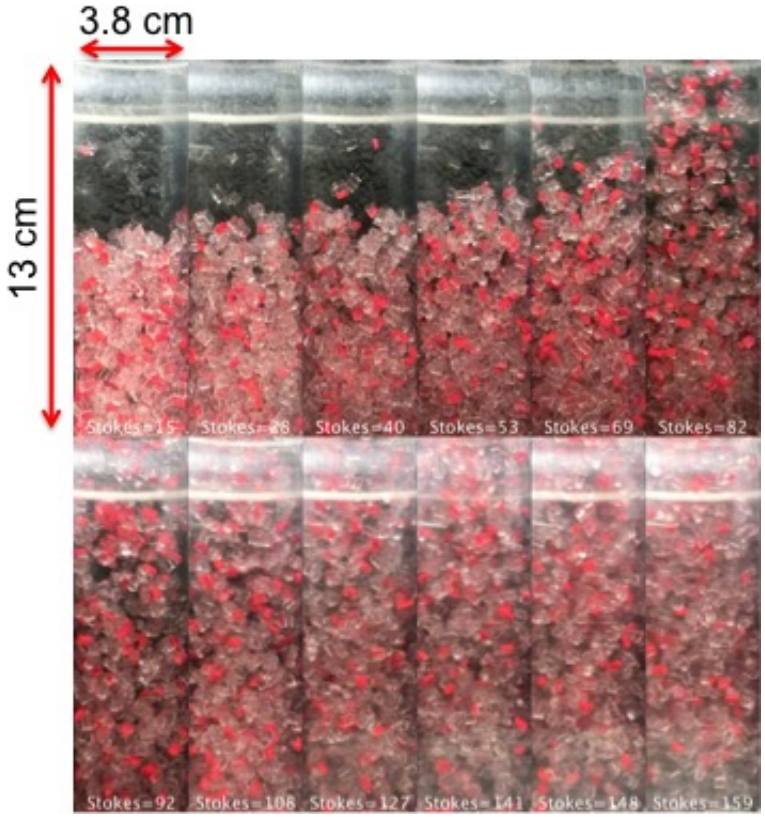


(a)

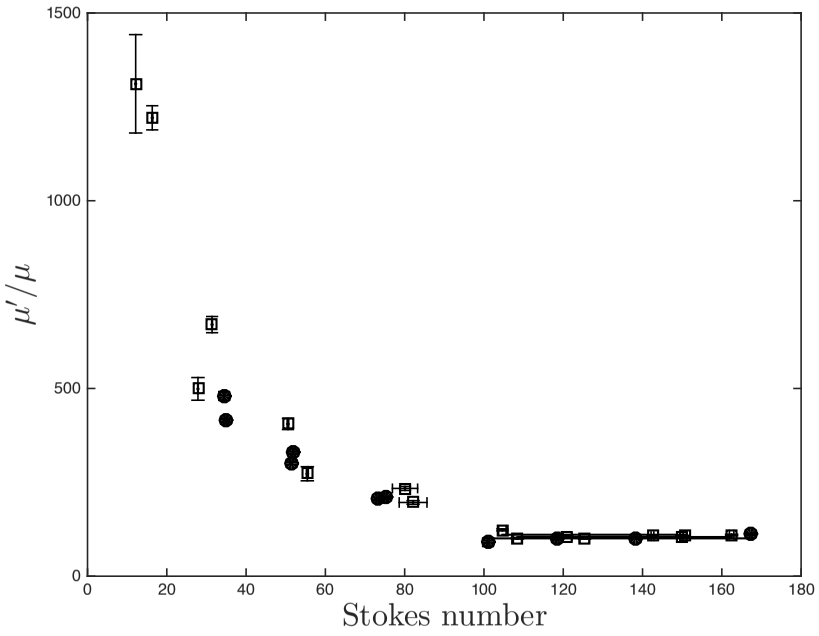


(b)

Figure 7.24: (a) Image sequence of flow over porous media with a loading fraction of 20% for different Stokes numbers. The height of the visualization window is the same as the height of the inner middle cylinder where the torque measurements are taken. (b) Effective relative viscosity as a function of Stokes number for loading fraction of 20% over a porous media. Closed symbols correspond to measurements taken with increasing shear rate. Open symbols correspond to measurements taken from high to low shear rates. $\rho_p/\rho = 1.03$.

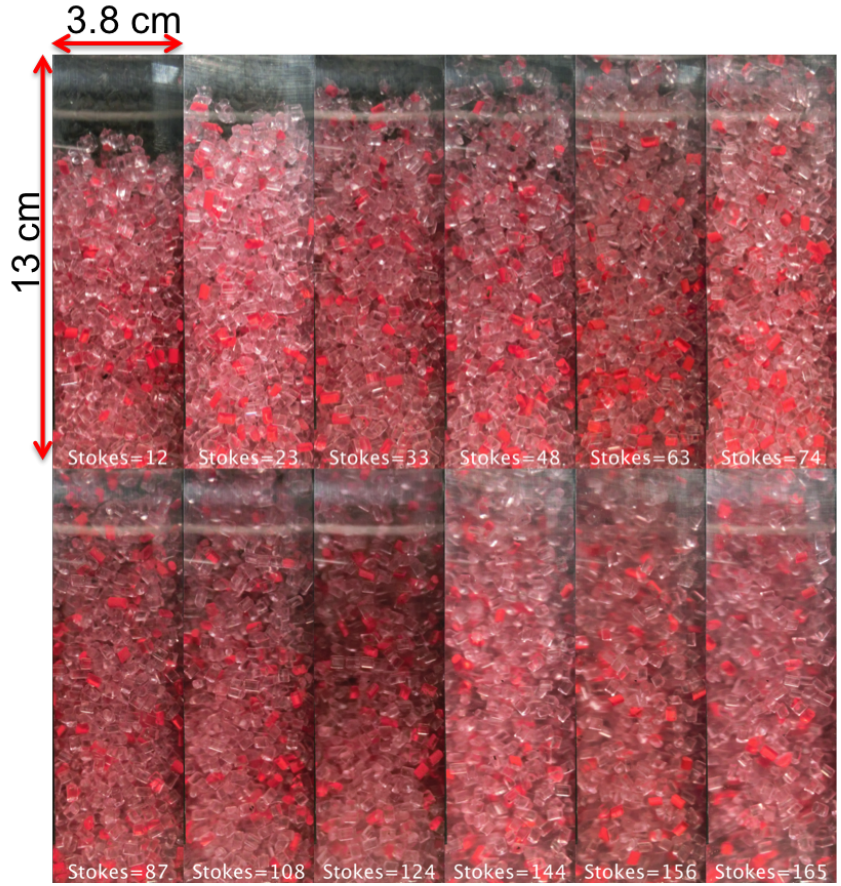


(a)

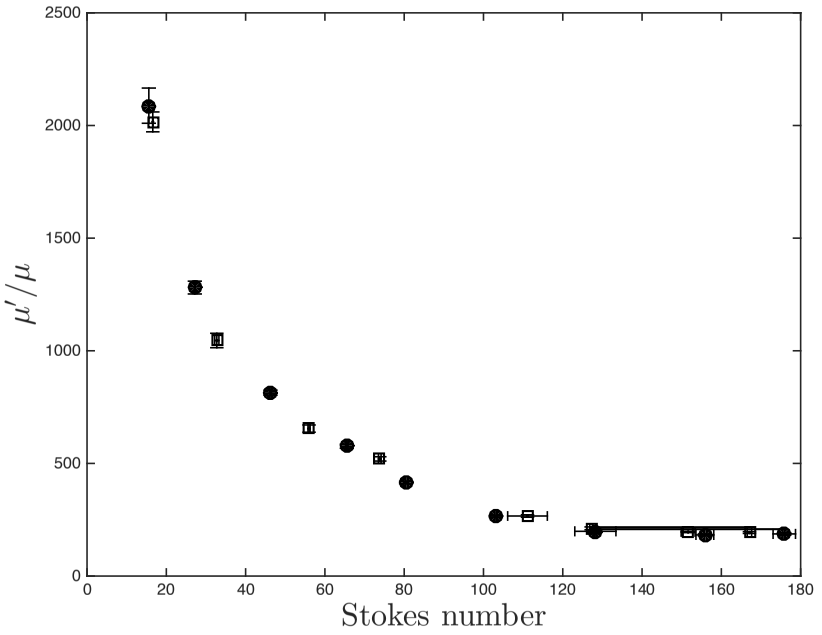


(b)

Figure 7.25: (a) Image sequence of flow over porous media with a loading fraction of 30% for different Stokes numbers. The height of the visualization window is the same as the height of the inner middle cylinder where the torque measurements are taken. (b) Effective relative viscosity as a function of Stokes number for loading fraction of 30% over a porous media. Closed symbols correspond to measurements taken with increasing shear rate. Open symbols correspond to measurements taken from high to low shear rates. $\rho_p/\rho = 1.03$.


(a)

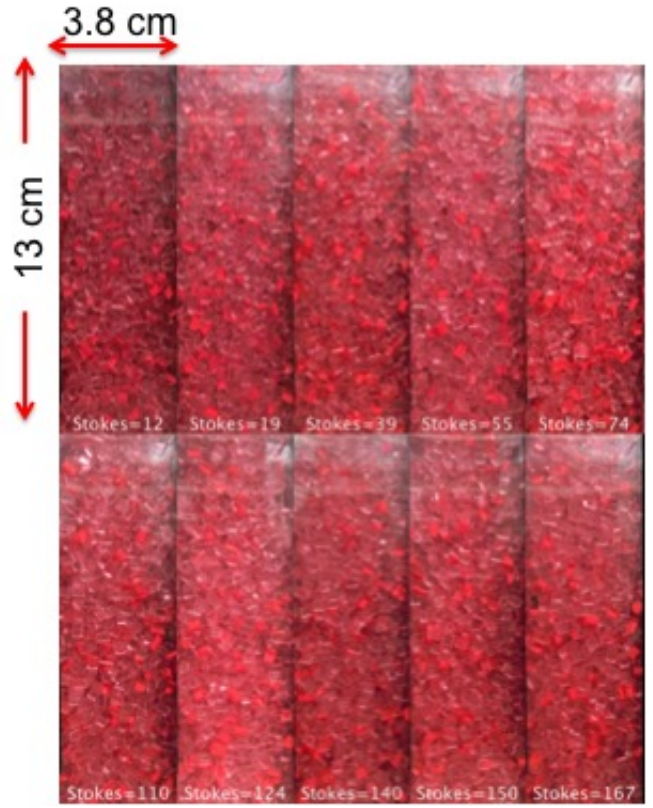


(b)

Figure 7.26: Image sequence of flow over porous media for different Stokes numbers. The height of the visualization window is the same as the height of the inner middle cylinder where the torque measurements are taken. (a) Loading fraction of 40%. (b) Loading fraction of 50%.

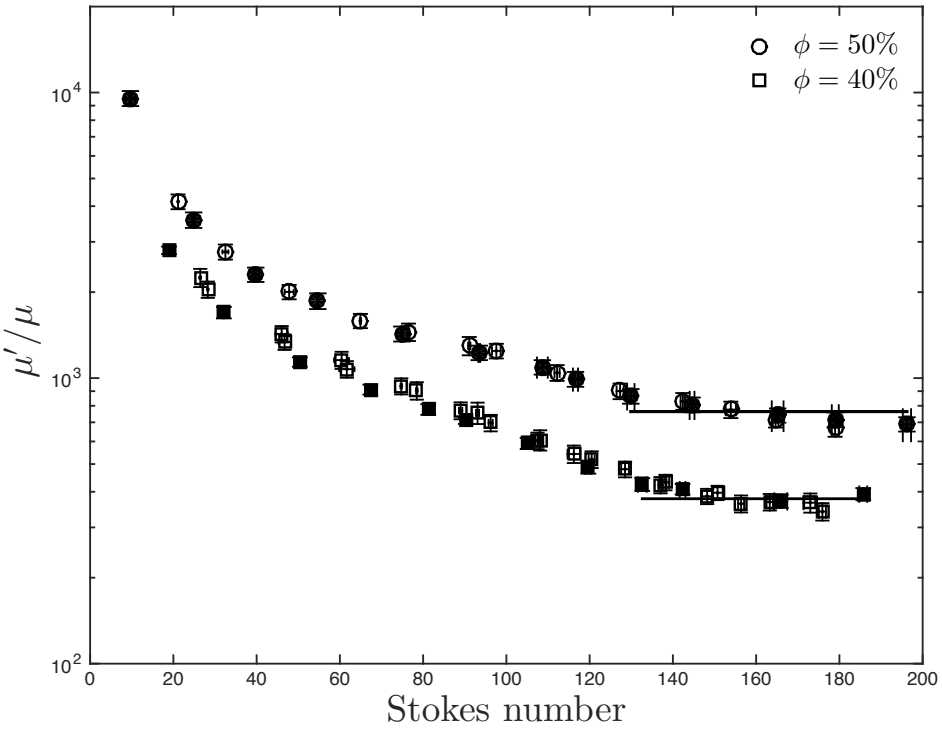


Figure 7.27: Effective relative viscosity for flow over porous media. Closed symbols correspond to measurements taken with increasing shear rate. Open symbols correspond to measurements taken from high to low shear rates. $\rho_p/\rho = 1.05$.

Stokes number corresponding to the cases where the particles cover the test cylinder completely are considered. The normalized torques for the flow over a porous media are higher than for the cases without a porous medium base. Figure 7.29 shows the normalized torques for the 3 cases studied:

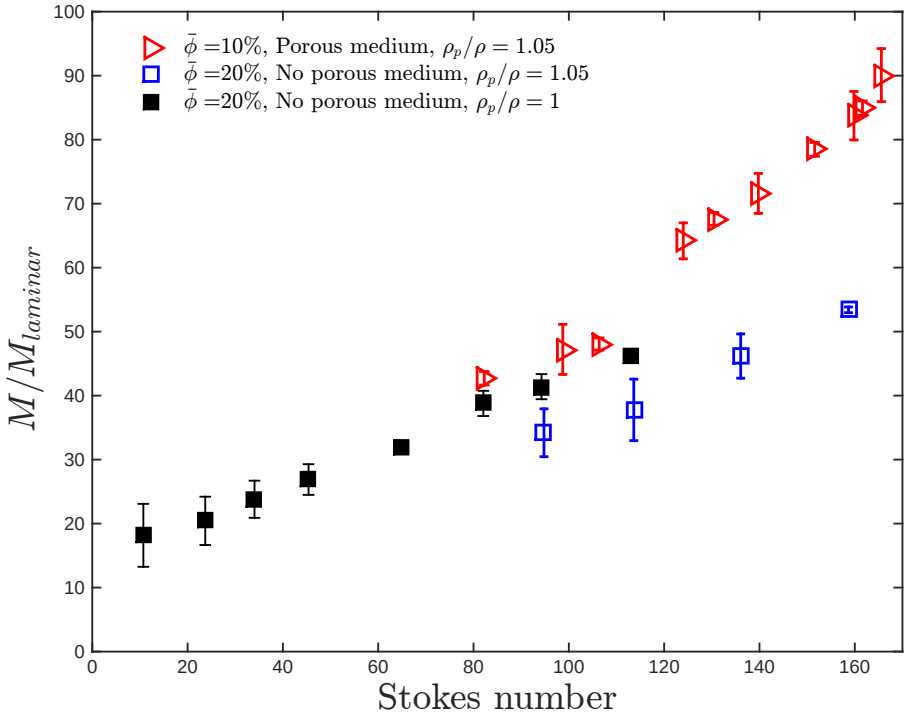


Figure 7.28: Flow over porous medium normalized torques as a function of St for $\bar{\phi} = 10$ compared with no porous medium with $\bar{\phi} = 20\%$ and $\rho_p/\rho = 1.05$ and $\rho_p/\rho = 1$. Only the data with no settling effects are considered.

$\rho_p/\rho = 1.05$, with and without bottom porous medium, and $\rho_p/\rho = 1$. The loading fraction for the flow over porous medium is 20% while the loading fraction for no porous medium is 30%. Only the case where the settling particles have reached the top of the annulus are considered. For the case with porous medium, this is considered to be at Stokes numbers where the normalized torques change in slope (see Figure 7.24). The cases without porous medium show a stronger dependance on the Stokes numbers than the case for the flow over a porous medium. However, the trend for these 3 cases is very similar. Figure 7.30 shows the normalized torques for a loading fraction of 30% with a porous medium and for a loading fraction of 40% for the case without it. The normalized torques for the flow over porous medium lie between the normalized torques for a $\bar{\phi} = 40\%$ with $\rho_p/\rho = 1.05$ and $\rho_p/\rho = 1$. The change in normalized torques dependance on Stokes number for the case with settling particles is considered to be linked to the fluidization of the particles. In the absent of hydrodynamics and particle interactions effects, a constant behavior of the normalized torques with the Stokes number would indicate a constant volume fraction. The results shown in Figure 7.30 suggest that the effective volume fraction for the case with a porous medium and $\bar{\phi} = 30\%$ is

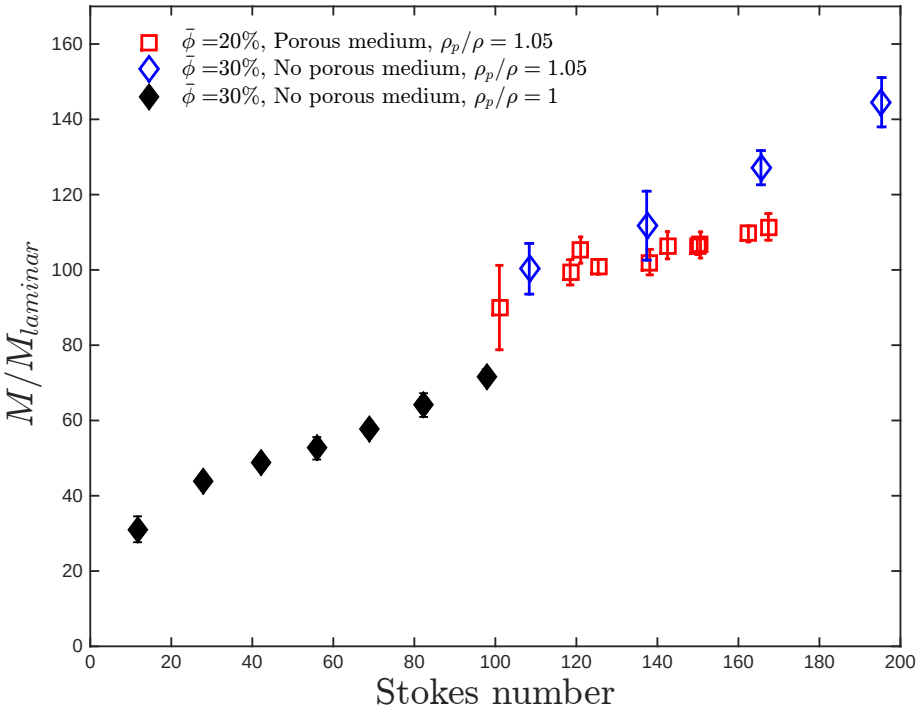


Figure 7.29: Flow over porous medium normalized torques as a function of St for $\bar{\phi} = 20$ compared with no porous medium with $\bar{\phi} = 30\%$ and $\rho_p/\rho = 1.05$ and $\rho_p/\rho = 1$. Only the data with no settling effects are considered.

higher than 40% (considering that the loading fraction for the case with matched densities is equal to the effective volume fraction), and that is less than the effective volume fraction for the case with settling particles and a loading fraction of 40%. In the next section a study of the effective volume fraction is presented to correct for the differences in loading and effective volume fraction. Lastly, Figure 7.31 shows the normalized torques for the three cases considered above with the normalized torques for a loading fraction of 40 and 50% for the flow over porous media, and 50% for the flow without it. As mentioned before, the normalized torques for the loading fraction of 50% decreases with Stokes number and did not become constant. However, by inspecting the measured torques, (see Figure 5.5), a drop occurs at shear rates around 60 $s^{-1}$, which corresponds to Stokes numbers around 100. In Figure 7.31 it is observed that the normalized torques for flow without the porous medium are more or less independent of the Stokes numbers. For the case with porous medium, the normalized torques continue to decrease with Stokes number. This indicates that the effects of settling (decreasing of the normalized torques with Stokes number) are more pronounced than for the case with porous medium. Therefore, even when the top particles have resuspended and touch the top section of the rheometer, the middle section of the column of particles have not been effectively fluidized. This suggests that the presence of the porous medium enhances the effects of a volume fraction gradient in the vertical direction. It is possible that in the absent of porous media,

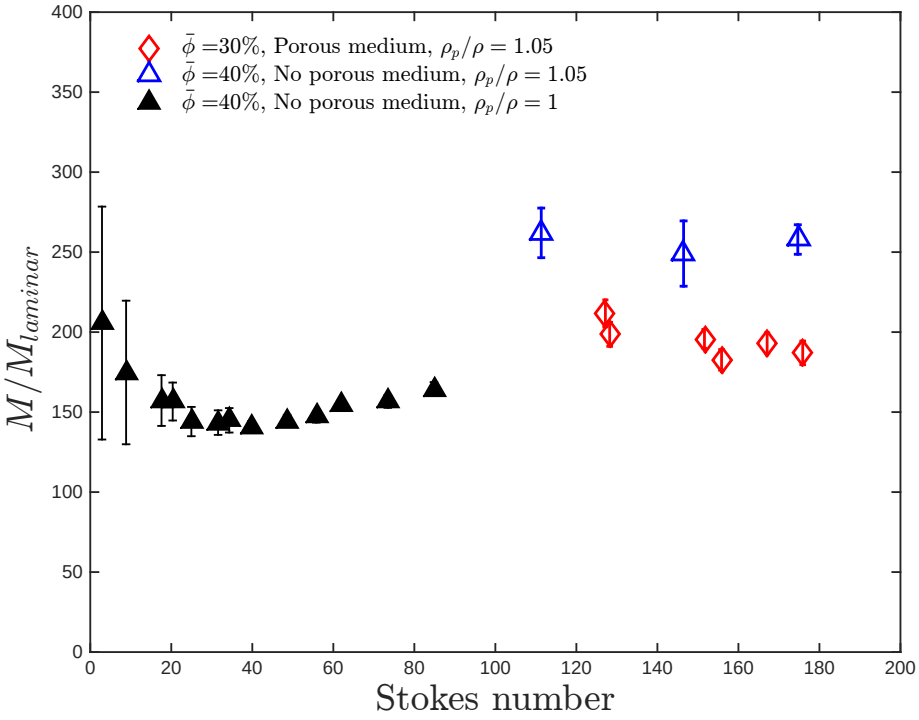


Figure 7.30: Flow over porous medium normalized torques as a function of St for $\bar{\phi} = 30$ compared with no porous medium with $\bar{\phi} = 40\%$ and $\rho_p/\rho = 1.05$ and $\rho_p/\rho = 1$. Only the data with no settling effects are considered.

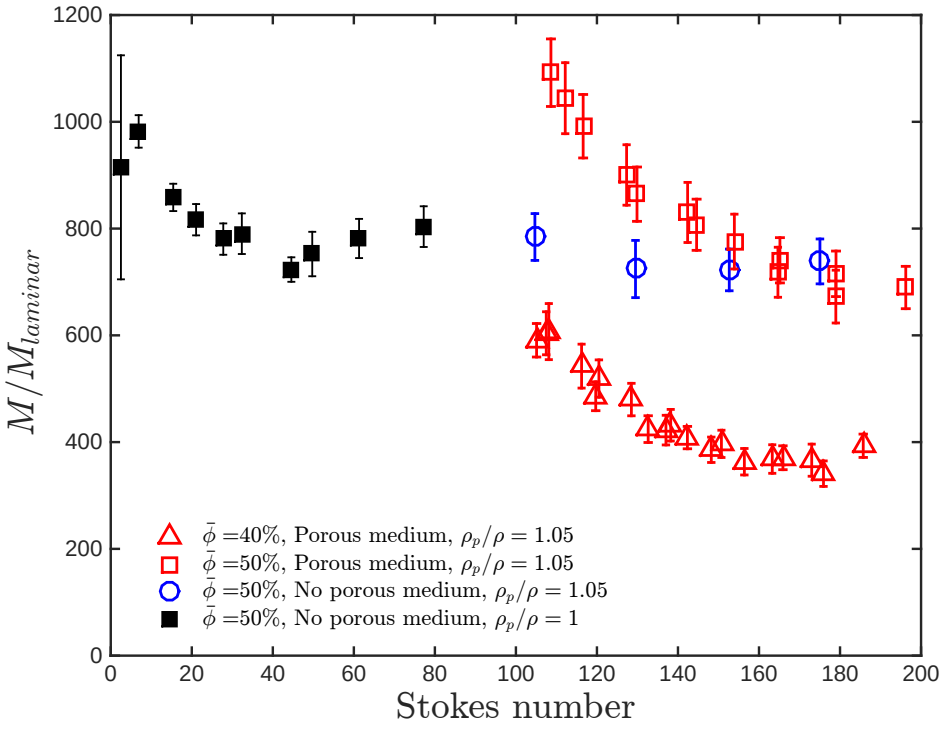


Figure 7.31: Flow over porous medium normalized torques as a function of St for $\bar{\phi} = 40$ and 50% compared with no porous medium with $\bar{\phi} = 50\%$ and $\rho_p/\rho = 1.05$ and $\rho_p/\rho = 1$. Only the data with no settling effects are considered.

the formation of secondary flows at the bottom helps fluidized the settling particles; meanwhile, the presence of porous media might weaker this effect.

### Effective volume fraction prediction for flow over a porous medium with $\rho_p/\rho = 1.05$

The effective volume fraction for the settling particles is inferred from the particle resuspension measurements that are described in Chapter 6. Using the same method described in Section 7.3, the effective volume fraction is estimated from the expansion results. However, due to the limited view of the visualization window used for these experiments, measurements of the height at high Stokes number are not possible. By comparing the measure heights normalized with the total height for the cases with and without a porous medium, similarities between certain loading fractions are found. Figure 7.32 shows the normalized measure heights for the case without porous medium and loading fractions of 20, 25, and 30 % compared with the normalized measure heights for flow over porous medium with loading fractions of 10, 20, and 30%. The normalized measure heights for the case

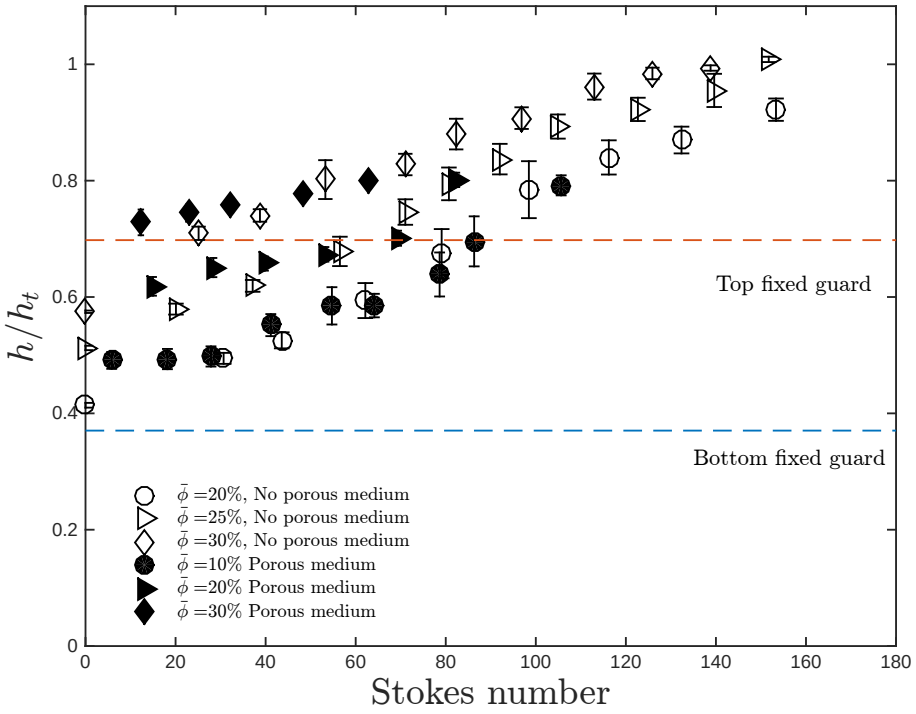


Figure 7.32: Particles normalized heights for flow with and without porous medium. The height is measured from the bottom of the annulus and normalized by the annulus total height.

with glass beads at the bottom seem to coincide with the heights corresponding to a higher loading fraction when no porous medium is placed. The effective volume fraction can then be inferred for a wider range of Stokes numbers by using the expansion for which the measured normal heights

seem to coincide. To test this method, the effective volume fraction is also predicted using linear extrapolation from the height measured for the limited Stokes numbers. Both methods lead to similar effective volume fractions. Figure 7.33 shows the effective relative viscosity as a function of the effective volume fraction for different Stokes numbers tested for $\rho_p/\rho = 1.05$. In here only the cases where the test cylinder is fully covered are considered. The magnitude of the Stokes numbers is represented with different sized symbols (the larger the Stokes number, the larger the symbol). The effective relative viscosity increases with volume fraction and for a loading fraction of 10% an

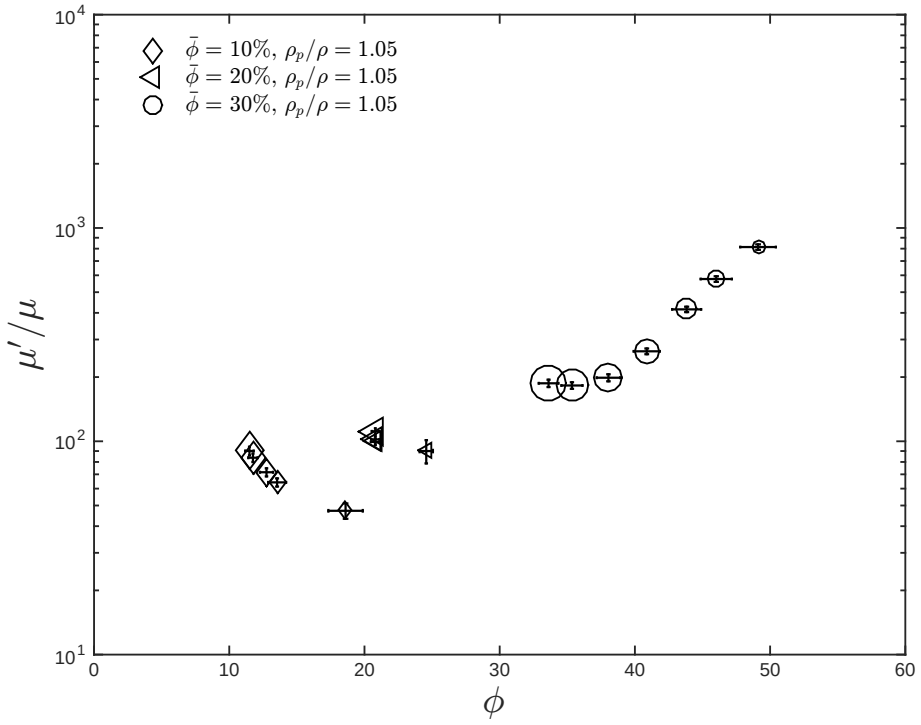


Figure 7.33: Effective relative viscosity for flow over porous media as a function of the effective volume fraction. Only the data where the test cylinder is fully covered are considered.

effect on the Stokes number is observed. For this particular case, the larger the St, the higher the effective relative viscosity and the lower the effective volume fraction is.

Comparisons between the case with settling particles but no porous medium are shown in Figure 7.34. The effective relative viscosity is higher for the case with a porous medium for volume fractions lower than 30%. For higher volume fractions the effective relative viscosity appears to coincide for both cases presented. Figure 7.35 shows the comparison between the three cases studied. With the exemption of the low volume fractions with a porous medium, the effective relative viscosity for all the other scenarios considered seem to coincide and follow the same trend. The differences in effective relative viscosity for low volume fractions seem to indicate the presence of a gradient in the volume fraction in the vertical direction. This gradient is more evident for the case with flow over a porous medium.

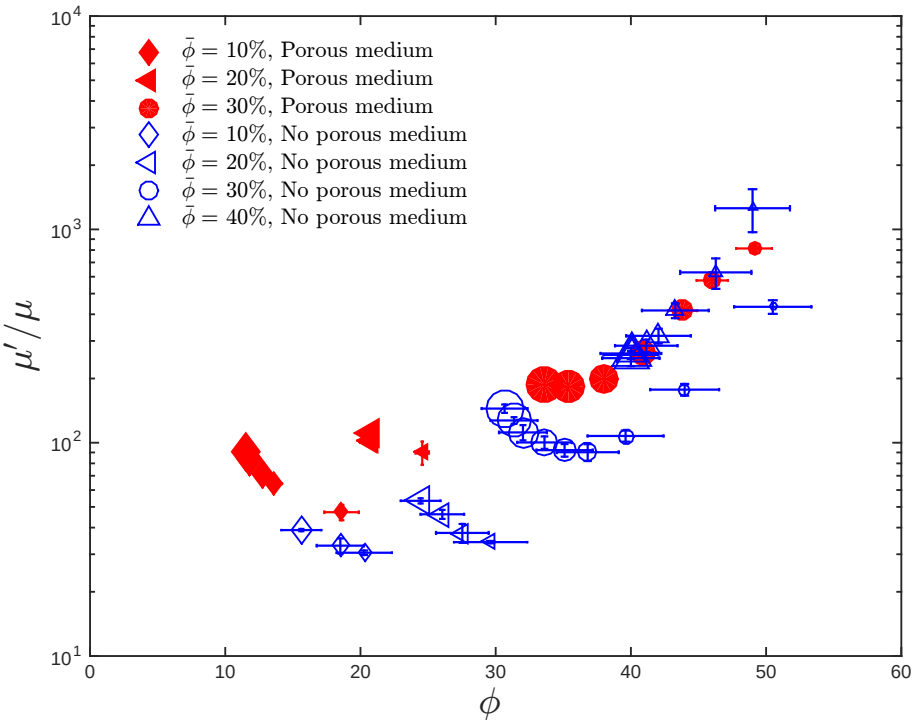


Figure 7.34: Effective relative viscosity as a function of the effective volume fraction for flow with and without porous medium. Only the data where the test cylinder is fully covered are considered.

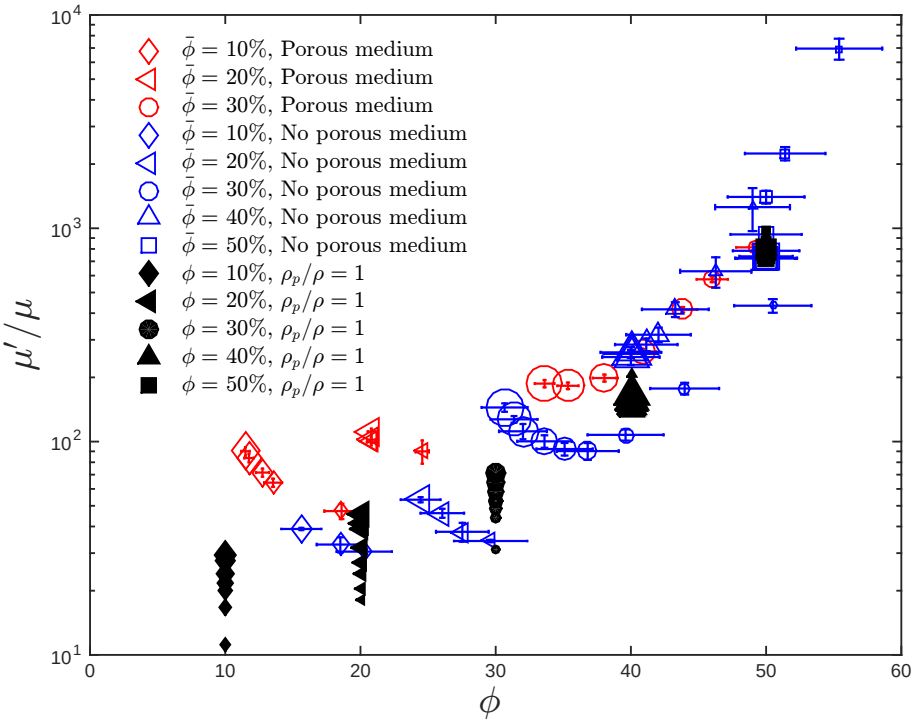


Figure 7.35: Effective relative viscosity as a function of the effective volume fraction for flow with and without porous medium with different density ratios. Only the data where the test cylinder is fully covered are considered.

### Inertial and particle concentration effects on flow over a porous medium with $\rho_p/\rho = 1.05$

Similar to the analysis done in Section 7.4 and 7.1, the effective viscosity of the mixture ($\mu'_{min}$) is inferred using the predicted effective volume fraction and Figure 7.3. The values of $\mu'_{min}$ are used to calculate the effective laminar torque ($M_{effe,\,laminar}$) and the effective gap Reynolds number ($Re_{b,\,effe}$). The measured torques normalized with the effective laminar torque as a function of the effective gap Reynolds number are presented in Figure 7.36 and compared with the different density ratio cases without porous medium. As considered for the cases without porous medium, only the data for Stokes number without settling effects are considered.

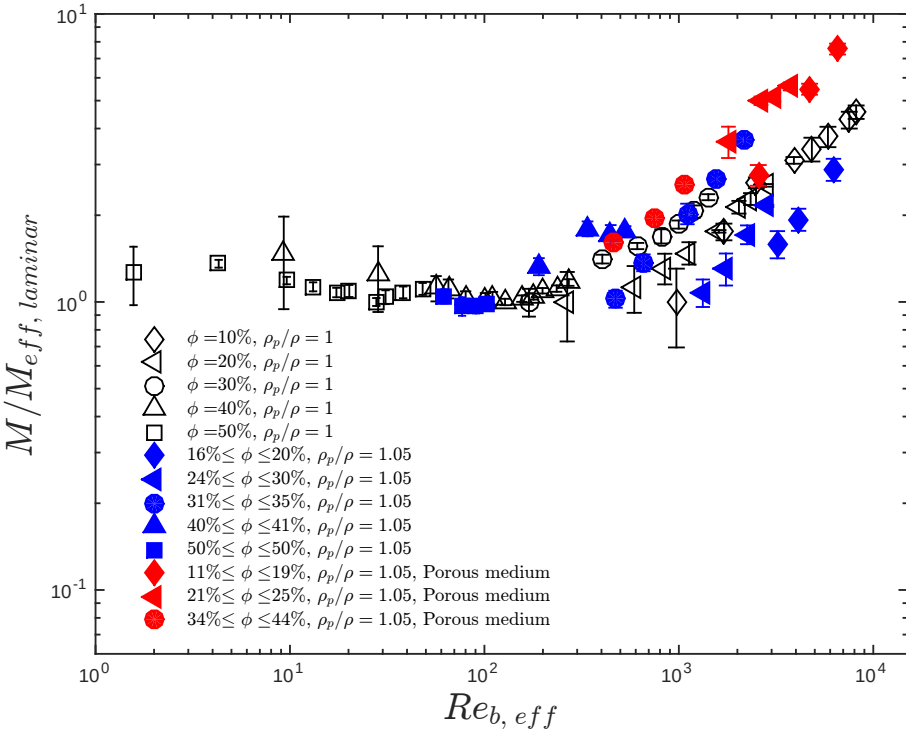


Figure 7.36: Measured toques normalized by the effective laminar torques as a function of the effective Reynolds numbers for $\rho_p/\rho = 1$ and $\rho_p/\rho = 1.05$ with and without porous medium. The effective viscosity of the suspension is inferred from the predicted effective volume fraction and Figure 7.3.

The normalized torques using the predicted effective viscosity are higher for the flow over a porous medium. As mentioned before, using Figure 7.3 to infer the value of the effective viscosity $\mu'_{min}$ introduces the uncertainties involved in estimating the effective volume fraction. If $\mu'_{min}$ is instead considered to be equal to the minimum value of $\mu'/\mu$ found for each loading fraction, then the scatter found in Figure 7.36 is reduced, as shown in Figure 7.37. For all the cases shown, the deviation from the laminar behavior occurs at the range of effective Reynolds number where the

pure fluid torque measurements are higher than the ones predicted from laminar theory.

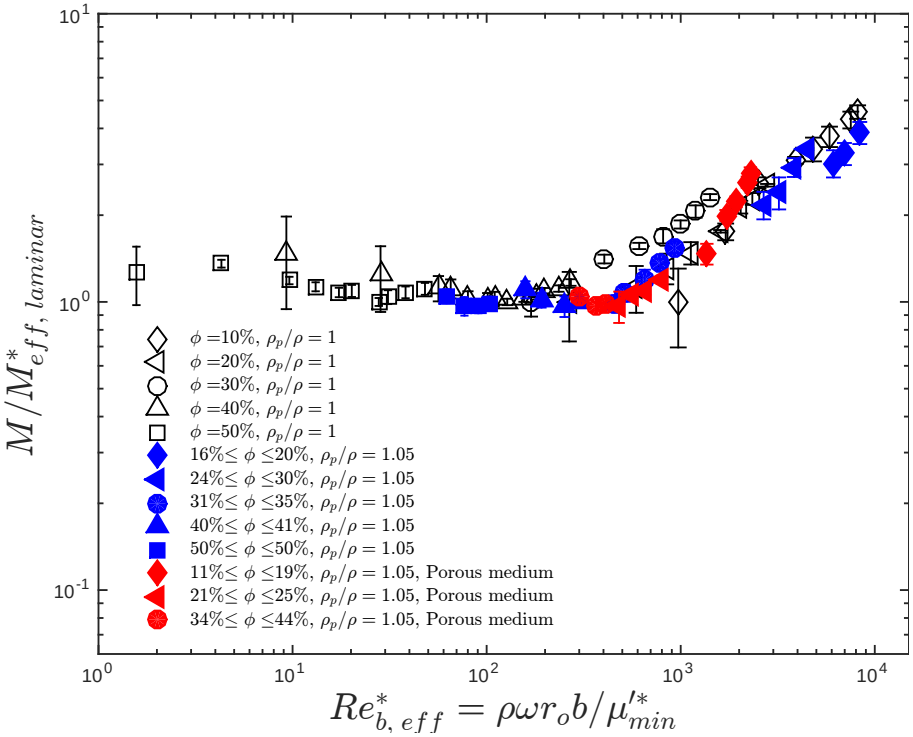


Figure 7.37: Measured toques normalized by the effective laminar torques as a function of $Re^*_{b,\ eff}$ for $\rho_p/\rho = 1$ and $\rho_p/\rho = 1.05$ with and without porous medium. The effective viscosity of the suspension is considered to be the minimum of the ratio $\mu'/\mu$ for each loading fraction.

## 7.6 Corrected torque for partial filling

As mentioned before in Section 7.2, for settling particles at low loading fractions and below a certain Stokes number, the particles do not cover entirely the test cylinder. To compare between these low loading fractions and the low loading fractions with $\rho_p\rho = 1$, a correction of the measured torques is needed. Such correction should take into account just the area covered by the liquid-solid mixture. This can be achieved by formulating that the measured torque is the sum of the contribution of the mixture and the contribution of the fluid, which leads to the following relation:

$$M = \tau 2\pi r_i^2 h_f + \tau_{mix} 2\pi r_i^2 h,$$

where $M$ is the measured torque, $\tau$ is the fluid shear stress , $\tau_{mix}$ is considered to be the shear stress applied by the liquid-solid mixture, and $h_f$ and $h$ are the height from the test cylinder covered by just the fluid and the mixture, respectively. The torque corresponding for just the mixture can be

obtained from equation 7.39 by considering that the fluid shear stress is equal to

$$\tau = \frac{M_f}{2\pi r_i^2 h_{test}},$$

where $M_f$ is the measured torque for just the fluid and $h_{test}$ is the height of the test cylinder. Since $M_f$ was measured for a limited range of gap Reynolds number, a curve fit from these measurements is used to infer the corresponding values of $M_f$ for higher Reynolds numbers. Figure 7.38 shows in a log log scale the pure fluid measured torque together with the curve fit used to infer the values of $M_f$ for plain water and the aqueous glycerine mixture of 21% used for the case with matched liquid density.

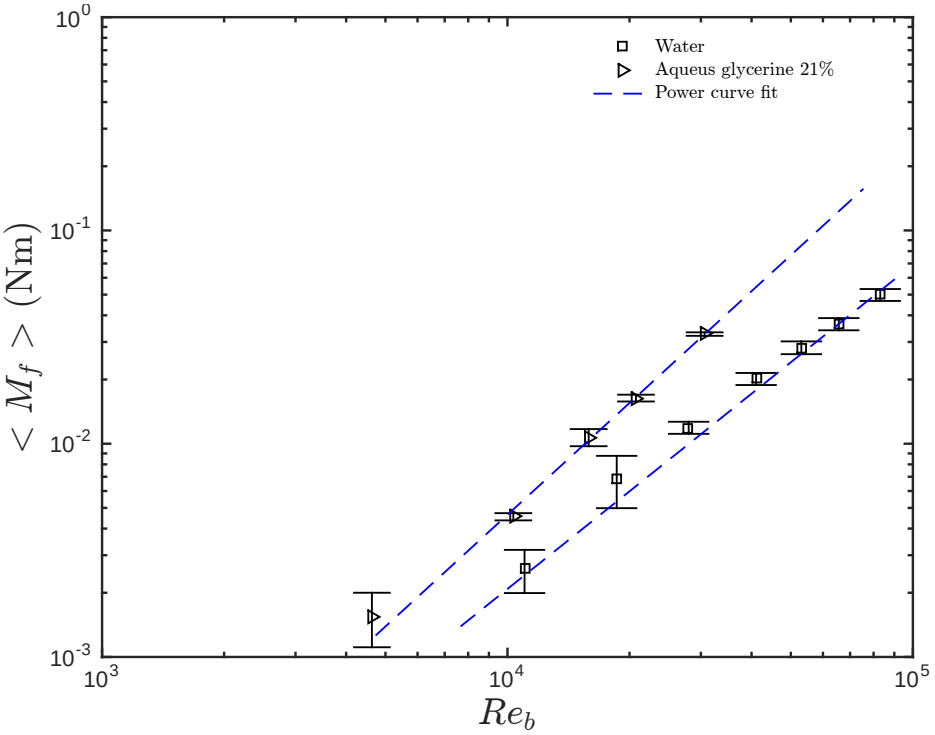


Figure 7.38: Measured torque for pure fluid as a function of gap Reynolds number and its curve fit presented in a log-log scale.

By substituting equation 7.6 into 7.39, the corrected torque for the mixture is

$$M_{mix} = M - M_f \frac{h_f}{h_{test}}, \tag{7.1}$$

where $h_f$ is equal to $h_{test} - h$. Figure 7.39 shows the corrected measured torque for volume fractions of 10 and 20% with $\rho_p/\rho = 1.05$. The correction applies only to the shear rates for which the liquid-solid mixture is only partially covering the test cylinder. For shear rates where the height predicted using the particles height measurements (discussed in Chapter 6) is above the test cylinder height,

$M_{mix}$ is considered to be equal to the measured torque ($M$). The torques for the shear rates where the test cylinder is partially covered, ($\dot{\gamma} < 80\ s^{-1}$ for $\bar{\phi} = 10$ and $\dot{\gamma} < 60\ s^{-1}$) does not show a strictly linear dependance with the shear rate, although there are not a significant number of measurements to determine the trend (for $\bar{\phi}$=10%, only 3 points were measured and for $\bar{\phi} = 20\%$ only 4). There is a jump between the corrected torques and the corresponding measured torque for the case where the particles fully cover the test cylinder. This might suggest that the contribution from the fluid to the measured torque is over-estimated during the correction or that the full resuspension of the particles increases the torque abruptly.

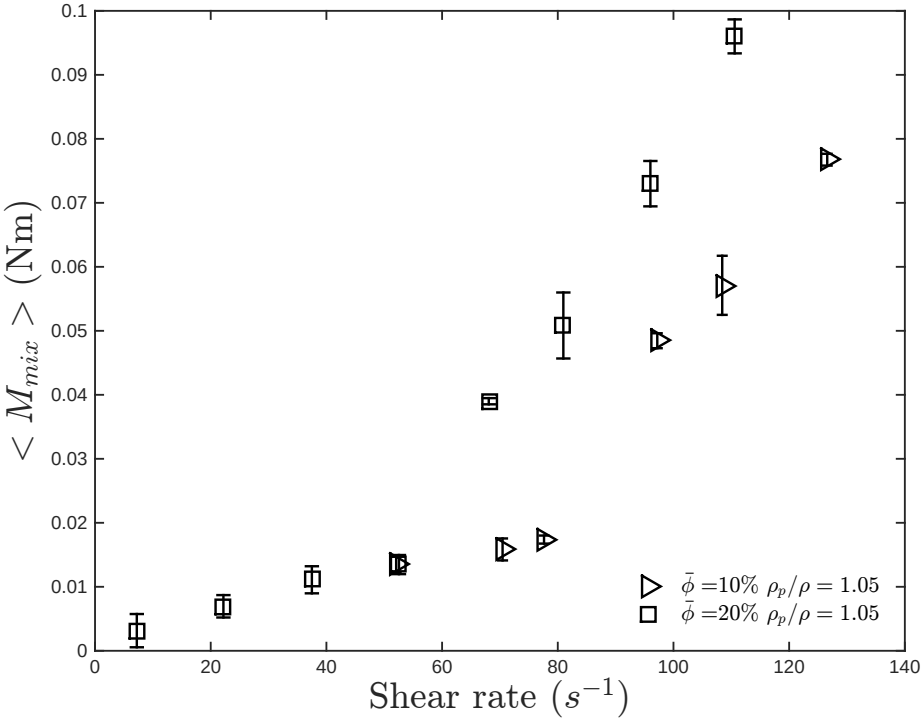


Figure 7.39: Corrected torque as a function of shear rate for partially covered test cylinder.

As mentioned before, it is possible that for these diluted mixtures, the contribution of the liquid might be stronger than for higher solid fractions. The presence of particles might not be strong enough to reduce the effective Reynolds number of the suspension. In such case, the contribution to the torque from the suspending liquid might be closer to the value measured for just the fluid. Figure 7.40 shows the corrected torque normalized by the theoretical laminar torque as a function of the Stokes number. The normalized torques for the Stokes for which the particles are partially covered are more scattered. When the test cylinder is fully covered, the normalized torques fluctuate less. For a loading volume fraction of 10% and 20% , the normalized torques increase with Stokes numbers when the test cylinder is fully covered.

Figure 7.41 shows a comparison between the normalized torques for $\rho_p/\rho = 1.0$ and $\rho_p/\rho = 1.05$. For the case with settling particles, the torques have been corrected to account when the test cylinder

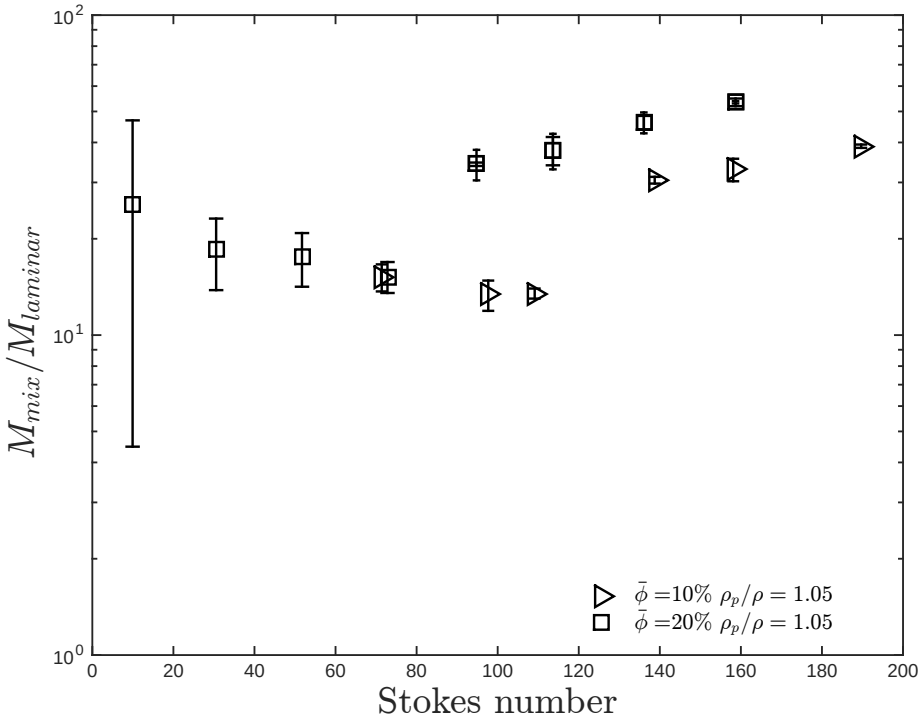


Figure 7.40: Corrected torque normalized by $M_{laminar}$ as a function of Stokes numbers.

is partially covered ($M_{mix}/M_{laminar}$).

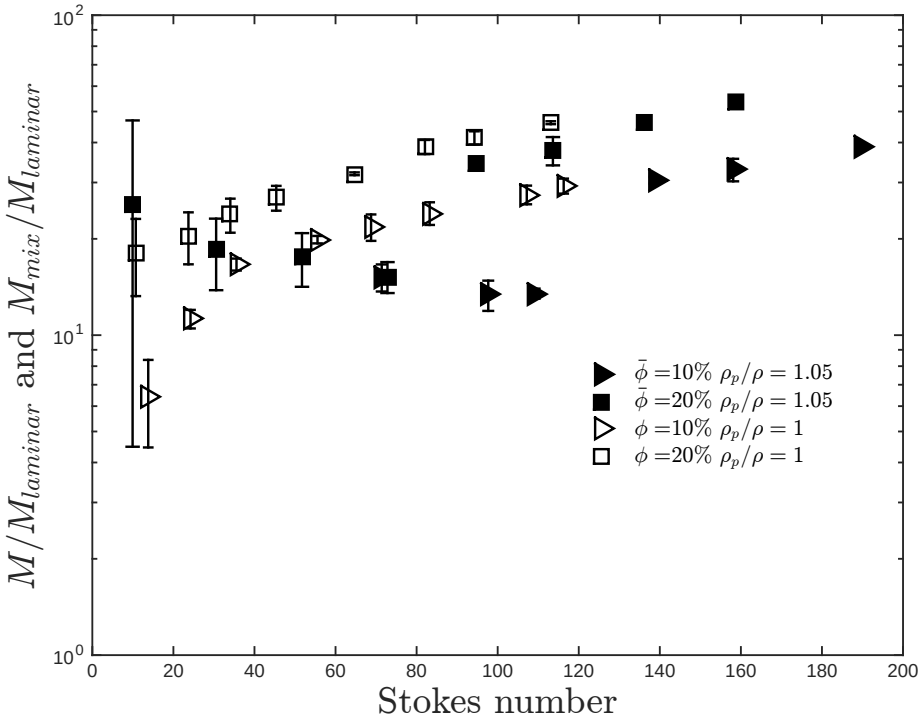


Figure 7.41: Corrected torque normalized by $M_{laminar}$ as a function of Stokes numbers compared with the data for $\rho_p/\rho = 1$.

For the case with $\rho_p/\rho = 1.05$, the normalized corrected torques for a loading fraction of 20% decrease with Stokes number, and once the particles fully covered the cylinder the corrected normalized torque increases. A similar behavior is found for a loading fraction of 10%. For this loading fraction only the data corresponding to the Stokes number where particles were present in the test section are considered. The correction of the torque when the test cylinder is partially covered does not seem to coincide with the measured torques for fully covered. This suggests that either the predicted height or the predicted pure fluid torque considered is not completely adequate.

## 7.7 Comparison between current and previous experimental and numerical results

The effective relative viscosity for the current and previous experiments of inertial suspensions is shown in Figure 7.42. For the current experiments with settling particles, the relative effective viscosity is plotted against the predicted volume fraction normalized by the particles random loose packing measured by Koos et al. (2012) ($\phi_{RLP} = 55.3\%$). Only the previous experiments with rough walls and Stokes numbers higher than $10^{-1}$ are compared. The empirical model used by Zarraga et al. (1999) is also shown in Figure 7.42 to compare the non-inertial results. The current experiments exhibit higher effective relative viscosities than the previous experimental work. Most of the experimental work of Prasad and Kytömaa (1995) correspond to Stokes numbers lower than the present study ($3.2 \times 10^{-2} \leq St \leq 3.2$) and their measurements involved settling particles with higher density ratio ($1.12 \leq \rho_p/\rho \leq 2.09$). Their torque measurements were made on the top of their annular shell and the suspension was sheared at the bottom at low shear rates. Such conditions could lead to lower effective volume fractions since the suspension is not sheared fast enough for the particles to fluidize. Similarly to Prasad and Kytömaa (1995), the density ratios for the experiments of Hanes and Inman (1985) are higher than for the present study ($2.48 \leq \rho_p/\rho \leq 2.78$) and the torques were also measured on the top surface. Unlike the work of Prasad and Kytömaa (1995), Hanes and Inman (1985) considered high shear rates. However, even when these experiments consider high shear rates, the complete fluidization of the particles may have not be achieved due to the higher density ratio which could lead to lower effective volume fraction than the one reported, and therefore lower effective relative viscosities.

As shown in Section 7.2, the effective relative viscosity for volume fractions higher than 30% showed no dependance on Stokes numbers as long as the particles are completely fluidized. Moreover, at these higher volume fractions, the hydrodynamic inertial effects were not present according to the analysis done in Sections 7.1 and 7.4. It is not clear then why the relative effective viscosity for these experiments is approximately one order of magnitude higher than the effective relative viscosity for the non-inertial suspensions. One possible explanation could be that at higher Reynolds numbers

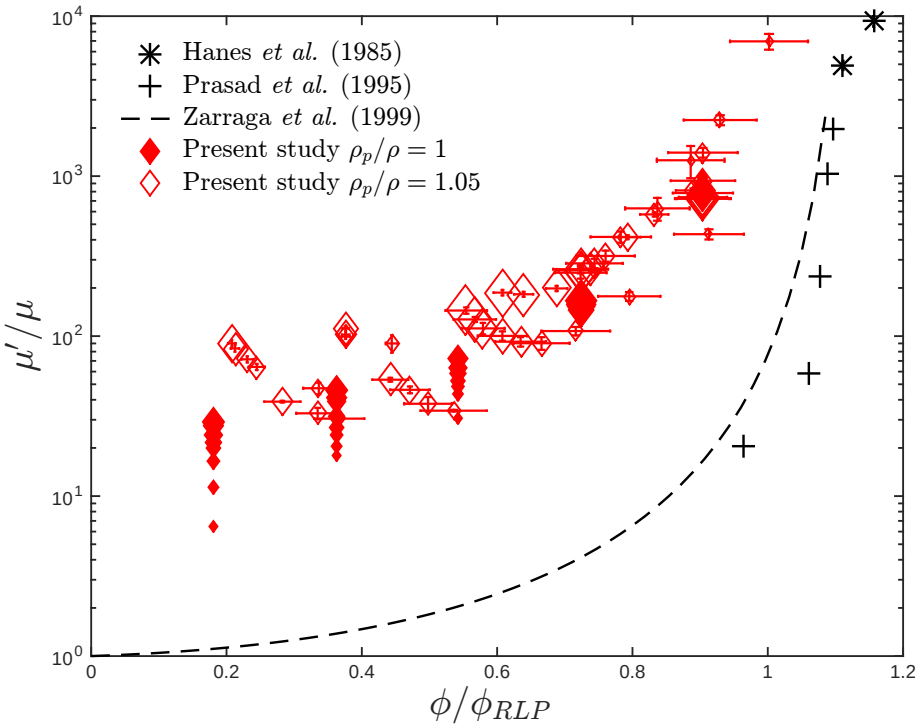


Figure 7.42: Effective relative viscosity as a function of volume fraction normalized by random loose packing for the present and previous experimental work. Only the previous experimental work with rough walls and Stokes numbers higher than one are presented. Dashed line corresponds to the empirical model proposed by Zarraga et al. (1999) to represent the results for non inertial suspensions. For the current results the size of the symbol represents the Stokes number magnitude.

the particle interactions increase and thus the velocity fluctuation of the flow. Velocity fluctuations lead to the presence of Reynolds stresses that are not present at low Reynolds number regimes. However, these Reynolds stresses increase with Reynolds number, leading to an increasing effective relative viscosity; however, the effective relative viscosity for these experiments show no dependance on Reynolds number. If Reynolds stresses are present for these experiments, then there must be a competing mechanism that balances the effect of increasing velocity fluctuations. It is not clear which mechanism could that be.

Figure 7.43 shows a comparison between the present study and the numerical results for suspensions with moderate Reynolds number. Only the current experiments with the lowest Reynolds numbers for each volume fraction is presented. The relative effective viscosity is plotted against the volume fraction normalized by the random loose packing. Since all the simulations considered spherical particles, the random loose packing used to normalized the volume fraction is calculated for monodisperse spherical particles using the fit of Zou and Yu (1996). Similarly to the comparison with previous experimental work, the present results show higher effective relative viscosities. For volume fractions lower than 30% the Reynolds number for the current experiments is approximately an order of magnitude higher than the Reynolds number considered in the simulations. The simulations of Kulkarni and Morris (2008) consider a Reynolds number range of $0.05 \leq Re \leq 16$, while the simulations of Picano et al. (2013) range the Reynolds number from $4 \leq Re \leq 40$ and the simulations of Yeo and Maxey (2013) consider lower Reynolds range of $0.02 \leq Re \leq 8$. The latest show the lowest relative effective viscosity even for the cases with the same volume fraction and Reynolds number. This discrepancy might be due to differences in their assumptions. Aside from using a different numerical method, Yeo and Maxey (2013) considered the Reynolds stress to be negligible. The later work of Haddadi and Morris (2014) showed that the contribution of the Reynolds stress to the bulk and particle-phase stresses is significant, therefore neglecting it would lead to lower effective relative viscosities which is consistent with the results showed in Figure 7.43.

Figure 7.44 shows the comparison between the effective relative viscosity as a function of Reynolds number for the present and numerical work of Picano et al. (2013) and Kulkarni and Morris (2008). Good agreement between the numerical simulations is shown. However, the present experimental work shows higher effective relative viscosities. A possible reason for this is the presence of slip at the wall observed in the work of Picano et al. (2013), where the ratio of particle velocity next to the wall and the wall velocity in their simulations is approximately 0.6. Similar velocity ratio was found in the smooth walls experiments of Koos (2009) for Reynolds numbers smaller than 100 and volume fractions below 40%. Such velocity ratio indicates the presence of slip and as shown by Barnes (2000) and Koos et al. (2012) it leads to lower effective viscosities. The relative effective viscosity for the current experiments for the lowest Reynolds number tested ($\mathcal{O}(100)$) are between 3 to 5 times higher than the numerical results of Picano et al. (2013) for Reynolds number equal to 40.

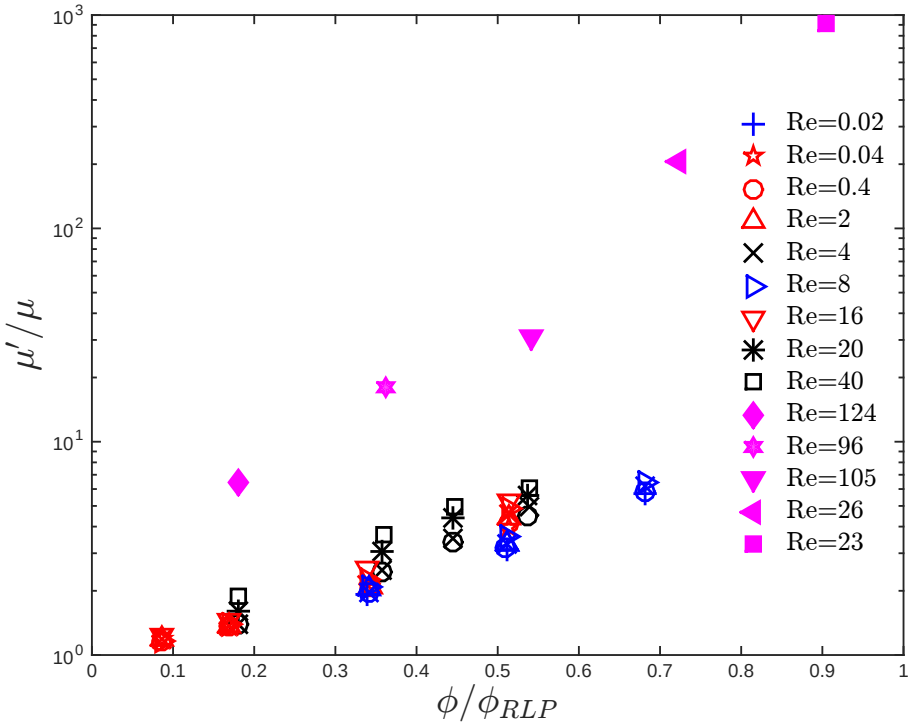


Figure 7.43: Effective relative viscosity as a function of volume fraction normalized by random loose packing for the present and previous numerical work. Solid symbols correspond to the present data. Blue symbols correspond to Yeo and Maxey (2013), red symbols correspond to Kulkarni and Morris (2008) and black symbols correspond to Picano et al. (2013).

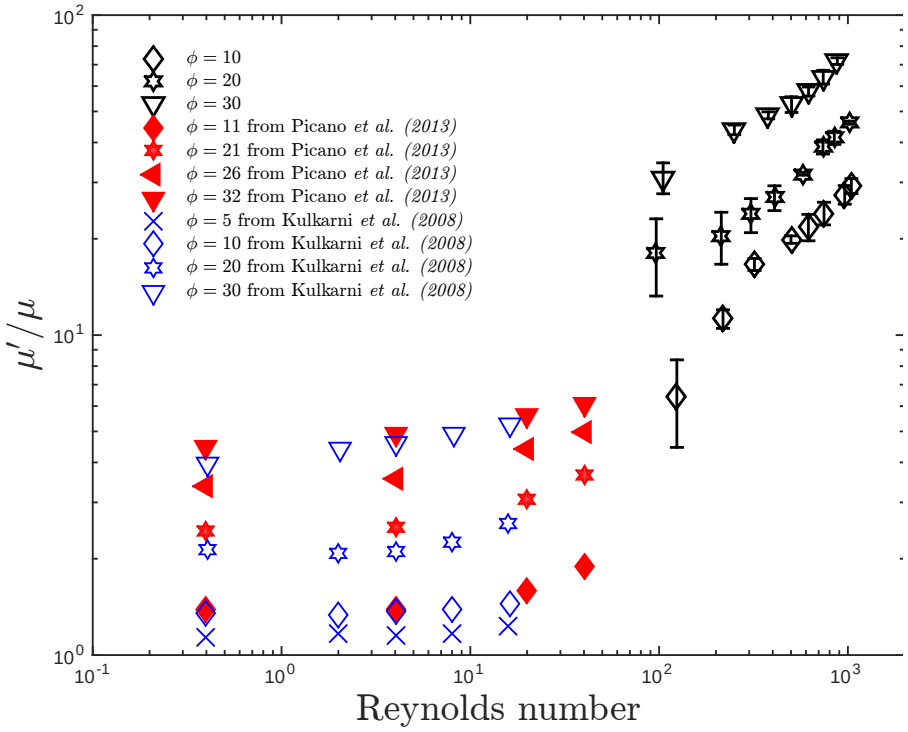


Figure 7.44: Effective relative viscosity as a function of Reynolds number for the present and previous numerical work. Black symbols correspond to the present data. Closed symbols correspond to Picano et al. (2013), red symbols correspond to Kulkarni and Morris (2008).

Based on the results of Koos et al. (2012), the effective viscosity can be up to 4 times higher than the apparent viscosity corresponding to experiments affected by slip at the wall for volume fractions lower than 40%.

A different mechanism occurs in the numerical work of Kulkarni and Morris (2008) where the particles tend to concentrate at the walls. The opposite behavior is observed experimentally, where the particles tend to move away from the wall. Kulkarni and Morris (2008) calculated the bulk stress and the stress at the wall, with the latest higher than the former. Because the particles are concentrating at the walls, there are less particles at the bulk, which would decrease the amount of particle interactions leading to lower effective relative viscosities.

## 7.8 Summary

Comparison between the cases of matched density and settling particles with and without a porous medium are presented.

Based on Figures 7.5, 7.22, and 7.37, the hydrodynamic inertial effects from the liquid seem only to be present for the dilute and moderately dilute liquid-solid mixtures. In the transition from laminar to turbulent flow in liquids, an increase in the liquid viscosity leads to a delay in

the transition regime because of the decrease in Reynolds number. It is unlikely that liquid-solid flows with low and moderate volume fractions would be an exception to this rule. As the volume fraction increases, the effective relative viscosity of the suspension increases considerably, leading to a decrease in effective Reynolds number of the mixture. For the three cases studied, the deviation from the laminar behavior occurs at an effective Reynolds number range that coincides with the region where the pure fluid measurements show a deviation from the laminar theory. This analysis is done by considering the data where the particles have been fluidized and where the effects of settling are weaker.

The effective volume fraction for the experiments with settling particles is predicted based on the results from the particle resuspension analysis (Chapter 6). When the effective volume fraction is considered, the relative effective viscosity for the case with $\rho_p/\rho = 1$ and $\rho_p/\rho = 1.05$ seems to coincide. This indicates that the effective relative viscosity is independent of the differences in density as long as the effective volume fraction is considered to correct for the presence of settling.

The experiments with a porous medium show higher relative viscosity at similar effective volume fraction. This suggests the presence of gradient in the volume fraction in the vertical direction. The presence of a lower base of heavier glass beads seems to affect the relative effective viscosity. The mechanism for this is still not clear.

Corrections to the measured torques for low loading fraction cases where the particles do not fully cover the test cylinder are presented considering that the contribution from the mixture and the suspending fluid can be obtained by inferring the height covered by the particles. The corrections do not seem to recover the shape of the normalized torques once the test cylinder is fully covered.

Comparison between the present and previous experimental and numerical work show that the effective relative viscosity for the current experiments are higher even for the cases where the inertial hydrodynamic effects are not present. The reason for this is not completely clear but possible reasons include a change in the effective volume fraction considered by the previous experimental work and presence of slip in the numerical simulations.